Journal of *Marine Science and Engineering*

MDPI

Article

Research on Dynamic Route Planning for Emergency Evacuation of Passenger Ships Considering Fire Spread

Kun Lang *, Xia Liu and Chunhui Niu

School of Maritime Economics and Management, Dalian Maritime University, Dalian 116026, China; 17863663390@163.com (X.L.); 15842674730@163.com (C.N.)

* Correspondence: kun.lang@dlmu.edu.cn

Abstract

To improve emergency response efficiency in passenger ship fire accidents and ensure the life safety of passengers and crew, this paper proposes a dynamic route planning model for passenger ship fire evacuation that accounts for fire spread. Firstly, a passenger ship fire spread model is established based on the field simulation theory, and an emergency evacuation network model is constructed by determining the evacuation network topology from the fire propagation process. Secondly, the factors affecting emergency evacuation route planning during fire spread are analyzed, and a multi-objective optimization model for dynamic evacuation routes is developed. Thirdly, an improved ant colony optimization algorithm is designed to solve the problem. Finally, using the RP1 vessel from the publicly available ship evacuation dataset of the EU Seventh Framework Program SAFEGUARD project as a case study, simulation and comparative experiments are conducted. The results show that, in medium- and large-scale evacuation problems, the proposed method consistently maintains higher computational efficiency compared with the DABD algorithm and the FOA. In terms of objective optimization, it demonstrates that the proposed method has better effectiveness and feasibility than the shortest-path evacuation strategy, as it minimizes evacuation cost while satisfying assembly station capacity constraints and achieves a more balanced utilization of all emergency exits.

Keywords: passenger ship fire; emergency evacuation; route planning; multi-objective optimization; ant colony algorithm

1. Introduction

Ship fires are one of the most serious safety threats in maritime transportation. According to the International Maritime Organization (IMO) accident database, among the 1202 maritime incidents recorded from 1 January 2020 to 1 June 2025, 71 were caused by ship fires [1]. Compared with fires in land-based buildings, ship fires are far more hazardous, as they are characterized by multiple ignition causes, rapid fire spread, great difficulty in fire suppression, and complex evacuation and rescue processes, thereby posing a serious threat to human life. In recent years, passenger ships have become a major choice for maritime transport and tourism [2]. In 2023, global passenger traffic exceeded 31 million. Therefore, when a ship fire occurs, carrying out effective emergency evacuation and minimizing casualties as much as possible is an urgent and complex task.

At present, research on emergency evacuation route planning for passenger ships under fire scenarios is relatively limited both domestically and internationally. Previous studies on passenger ship evacuation route planning have mostly treated the problem as a

Check for updates

Academic Editor: Vincenzo Crupi

Received: 17 May 2026
Revised: 28 June 2026
Accepted: 29 June 2026
Published: 1 July 2026

Copyright: © 2026 by the authors. Licensee MDPI, Basel, Switzerland. This article is an open access article distributed under the terms and conditions of the Creative Commons Attribution (CC BY) license.

static path planning issue within a certain scope, often neglecting the impact of various dynamic environmental factors during fire spread on evacuation route planning, and typically assuming that evacuees' movement speed is constant. In addition, the efficiency of the algorithms used to solve path planning models still needs to be further improved.

To address these issues, this study focuses on the dynamic evacuation route planning problem for passenger ships under fire spread scenarios, with the main contributions as follows:

(1) Construction of the passenger ship fire emergency evacuation network. The construction of the evacuation network is of great importance and serves as the foundation for the study of dynamic route planning for passenger ship fire emergency evacuation. In this paper, a passenger ship fire spread model is developed based on field simulation theory, including the turbulence flow model, combustion model, and radiative heat transfer model. Based on the fire spread process, the topological structure of the evacuation network is determined, and an evacuation network model is subsequently established.

(2) Construction of the dynamic route planning model for passenger ship fire emergency evacuation. First, the factors affecting emergency evacuation route planning during passenger ship fire spread are analyzed. Then, by comprehensively considering the effects of these factors on evacuation efficiency and safety, the real-time influence of various dynamic environmental factors during fire spread on evacuee movement speed is quantitatively evaluated. On this basis, a multi-objective optimization model for dynamic evacuation route planning under passenger ship fire conditions is established. Specifically, minimum evacuation time, minimum evacuation distance, and minimum fire risk are selected as the objective functions of the dynamic evacuation route optimization problem under time-varying conditions. Corresponding constraints are formulated in terms of route feasibility, unidirectionality, evacuation time, and assembly station capacity.

(3) Algorithm development for solving the dynamic route planning model for emergency evacuation in passenger ship fires. In this study, the model is solved using an improved ant colony optimization algorithm. The improvements include: (1) applying linear interpolation to fire environment parameters, such as carbon monoxide concentration, temperature, and visibility, to accurately estimate conditions at each evacuation node at any time; (2) designing a heuristic function that jointly considers multiple evacuation objectives; (3) introducing a non-dominated sorting-based multi-objective pheromone update mechanism to identify routes with better overall performance; and (4) adopting an adaptive backtracking strategy to prevent the algorithm from entering dead loops.

The remainder of this paper is organized as follows. The relevant literature is reviewed in Section 2. The passenger ship fire emergency evacuation network model is constructed in Section 3. The dynamic route planning model for passenger ship fire emergency evacuation is developed in Section 4. In Section 5, the RP1 vessel from the publicly available ship evacuation dataset of the EU Seventh Framework Program SAFEGUARD project is taken as a case study to conduct simulation and comparative experiments, thereby verifying the feasibility and effectiveness of the proposed model and algorithm. Finally, the conclusion is presented in Section 6.

2. Literature Review

In the optimization of passenger ship evacuation plans, issues like evacuation route planning and the timing of evacuation orders have attracted attention from researchers. For example, Casareale et al. [3] used a modified version of the FDS and EVAC Fire Dynamics Simulator to simulate ship evacuation scenarios, demonstrating the effectiveness of wayfinding solutions in improving passenger evacuation flows and route selection. Ng et al. [4] proposed a passenger ship evacuation model minimizing evacuation time,

considering various groups (children, women, elderly), and established an accelerated method for real-time emergency response, optimizing strategies for diverse evacuee groups and resources to meet operational demands. Xie et al. [5] proposed an agent-based optimization method for determining evacuation order timing, which identifies optimal and worst response time parameters while significantly reducing evaluation samples. Research on passenger ship evacuation optimization is still in its early stages, with few results, while studies in other evacuation fields are more abundant [6–11]. Although the research subjects differ, these studies all aim to enhance evacuation efficiency by considering resource allocation, safety, and time constraints, providing valuable insights for passenger ship evacuation research.

Unlike land-based buildings, passenger ships are floating transport systems whose evacuation processes are also affected by ship motions, such as heel, trim, and rolling, as well as marine environmental factors. Accordingly, some studies have examined how ship motion influences evacuation behavior [12–14]. However, what researchers have rarely considered is that smoke, toxic gas dispersion, and temperature exhibit significant time-varying characteristics in ship fire evacuation [15,16]. These dynamic factors can reduce route capacity, slow evacuees, prolong evacuation time, and ultimately affect overall evacuation efficiency [17]. However, existing studies usually formulate route optimization as a discrete network flow problem with time constraints [18], and relatively little attention has been paid to the real-time impact of sudden fire events on the time-varying capacity of evacuation links. Most studies assume that evacuees' movement speed remains constant on each link of the evacuation network. Therefore, ship evacuation modeling under fire scenarios should account not only for multiple optimization objectives but also for the dynamic evolution of the fire environment and its real-time impact on evacuation.

At present, research on dynamic route planning methods for ship passenger evacuation remains limited, although some progress has been made in other related fields. Some scholars have attempted to address dynamic shortest route problems by improving classical static shortest route algorithms such as Dijkstra and A* [19,20], but these methods still have limitations when dealing with complex multi-objective problems. With the advancement of science and technology and the integration of multiple disciplines, bio-inspired intelligent algorithms, such as artificial immune systems, genetic algorithms, and ant colony algorithms, have gradually been introduced into the field of dynamic route planning. These algorithms simulate natural biological behaviors or evolutionary mechanisms, providing new approaches to solving complex dynamic optimization problems. For example, Khalid et al. [21] addressed emergency route planning under disaster scenarios by characterizing crowd dynamics through group cohesion and applying an artificial immune system (AIS) algorithm to optimize routes. Zhang et al. [22] proposed an improved genetic algorithm for mobile robot route planning in dynamic environments by introducing visible space, matrix encoding, and new mutation operators, thereby enhancing solution feasibility and algorithm convergence speed. Men et al. [23] developed an adaptive chaotic particle swarm optimization algorithm to solve multi-crowd congestion-relief evacuation planning under Gaussian Type-2 fuzzy environments. Numerical experiments demonstrated that this method performed well in terms of solution quality and computational efficiency. Ant colony optimization (ACO) algorithms, due to their strong adaptability, prominent positive feedback mechanisms, and robustness, have been widely applied across various fields [24–27]. For instance, Li et al. [28] constructed an optimization model for multi-depot green vehicle routing aiming to maximize profit while minimizing cost, time, and emissions, and solved it using an improved ACO algorithm; the results showed superior solution quality compared to classical ACO. Deng et al. [29] developed a hybrid optimization algorithm combining multiple particle swarm strategies with ant colony optimization for

airport runway planning, demonstrating effective optimization of taxiing routes, reduced conflicts, and improved utilization of taxiway resources. Dong et al. [30] addressed dynamic evacuation route planning under dam-break flood scenarios by constructing a road network using graph theory and proposing a hybrid algorithm (ACO-GA) that combines a backtracking strategy, elite ant mechanism, and genetic algorithm advantages to overcome the slow convergence and local optima issues of traditional ACO. Results indicated that this hybrid algorithm outperformed the basic ACO in both accuracy and convergence speed. Liu et al. [31] proposed an improved ant colony system (IACS) to solve the emergency evacuation route planning problem for cruise ship crowds, and improved the algorithmic efficiency by introducing an increasing flow method, thereby verifying the applicability of ant colony algorithms to multi-route evacuation planning for cruise ships. These studies provide new ideas for solving dynamic evacuation route planning problems; however, existing algorithms still show insufficient adaptability to multi-objective, highly time-varying scenarios such as cruise ship fire evacuation in aspects including parameter handling, heuristic function construction, pheromone updating, and deadlock management.

In summary, at present, research on emergency evacuation route planning for passenger ships under fire scenarios is relatively limited both domestically and internationally. Previous studies on passenger ship evacuation route planning have mostly treated the problem as a static path planning issue within a certain scope, often neglecting the impact of various dynamic environmental factors during fire spread on evacuation route planning, and typically assuming that evacuees' movement speed is constant. In addition, the efficiency of the algorithms used to solve path planning models still needs to be further improved. Therefore, this study focuses on the dynamic evacuation route planning problem for passenger ships under fire spread scenarios.

3. Construction of the Passenger Ship Fire Emergency Evacuation Network

To clarify the overall methodological framework of this study and the logical relationship among the main research procedures, the technical roadmap of the proposed method is first presented in this chapter, as shown in Figure 1. The framework follows the logic of "evacuation network construction–fire spread simulation–dynamic route planning model formulation–multi-objective optimization solution". Specifically, in Section 3, the evacuation network under fire-affected conditions is established. In Section 4, the multi-objective dynamic route planning model based on this network is further developed and an improved ant colony optimization algorithm is designed.

In the study of dynamic route planning for passenger ship fire emergency evacuation, the construction of the evacuation network is of great importance, as it provides the foundation for route planning research. This section focuses on the development of the evacuation network, mainly including the network construction of the evacuation environment, the construction of the fire spread model, and the determination of the evacuation network topology based on the passenger ship fire spread model.

3.1. Evacuation Environment Network Construction

To meet the application requirements of the evacuation model developed in this study, the two-dimensional passenger ship layout must be transformed into an evacuation network topology. According to the functions of different onboard facilities, a passenger ship can be divided into areas such as bars, restaurants, stairways, shopping areas, cabins, storage areas, corridors, and decks. Some of these areas are connected by corridors or doors. Therefore, this study first takes the centroid of each area as a network node, and then determines the connectivity between different areas by identifying whether doors

or corridors exist between them. Finally, the centroids are connected through doors and corridors, and the accessible passageways linked to each centroid are treated as the edges of the network structure, thereby generating the evacuation network topology and converting the evacuation environment into a network representation.

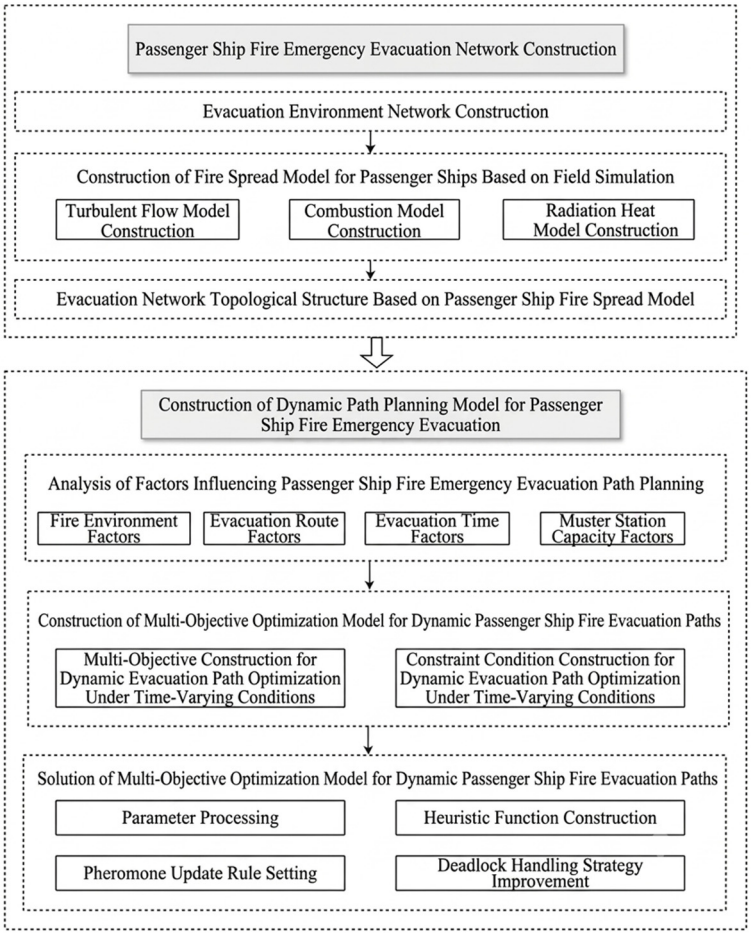


Figure 1. Technical roadmap.

Specifically, the emergency evacuation network is represented by a directed graph $G = (V, A)$, in which $V = V_s \cup V_d$, $V_s = \{v_s | s = 1, 2, 3, \ldots, n_s\}$ and $V_d = \{v_d | s = 1, 2, 3, \ldots, n_d\}$ denote the set of source nodes (i.e., the locations of evacuees) and the set of destination nodes (i.e., the evacuation exits of the passenger ship), respectively; i and j are node indices; and $A = \{(v_i, v_j) | v_i, v_j \in V\}$ denotes the set of arcs. The topology of the evacuation network is shown in Figure 2.



Figure 2. A network topology diagram.

3.2. Construction of Field Simulation-Based Passenger Ship Fire Spread Model

In this study, the passenger ship fire spread model is developed based on field simulation. In the field model, the entire passenger ship domain is divided into numerous small and discrete control volumes, as shown in Figure 3, where $A \sim G$ denotes the boundary point. Energy, mass, and chemical species are exchanged between adjacent control volumes through the nodes located on their boundaries, making it possible to obtain more realistic

distributions of the temperature field and smoke field, as well as accurate distributions of various physical quantities.

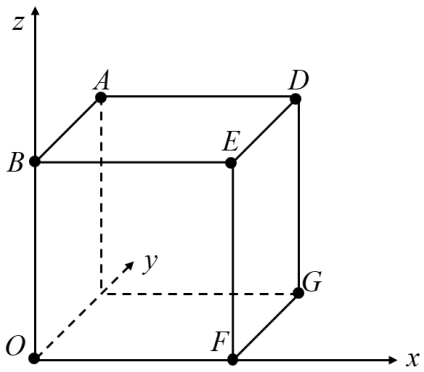


Figure 3. Control body.

Specifically, the exchanged energy, mass, and chemical species in the field model are the coupled products of different physical processes, and are mainly computed through three mathematical models: the turbulent flow model, the combustion model, and the radiative heat transfer model. These three models work in close coordination during field simulation, each providing the necessary data support for the others and jointly reproducing the complex dynamic behavior of fire. The turbulent flow model [32] is used to calculate the movement and diffusion routes of smoke in enclosed spaces under fire conditions. The combustion model [33] is used to simulate the combustion process of the fire and is responsible for generating the heat, smoke, and toxic gases produced during the fire. The radiative heat transfer model [34] is used to calculate the thermal impact of the fire on adjacent cabins and passageways.

3.3. Evacuation Network Topology Based on the Passenger Ship Fire Spread Model

During fire spread, smoke temperature, visibility, and CO concentration pose serious threats to evacuees' health. Therefore, this study selects smoke temperature, visibility, and CO concentration as the key parameters in the evacuation network, and calculates their values under time-varying conditions to evaluate the impact of fire spread on passenger evacuation.

First, the calculation of CO concentration involves the mass conservation equation and the chemical reaction kinetics equation. Specifically, the variation in CO concentration can be described by the following convection–diffusion–reaction equation:

$$\frac{\partial \rho_{co}}{\partial t} + \nabla \cdot (\rho_{co} u) = \nabla \cdot (D_{CO} \nabla \rho_{co}) + R_{CO} \quad (1)$$

where ρ_{co} is the concentration of CO (mass fraction or mole fraction), u is the fluid velocity vector, D_{CO} is the diffusion coefficient of CO, and R_{CO} is the generation/consumption rate of CO, which can be calculated using a chemical reaction kinetics model.

The chemical reaction kinetics model is usually expressed in the form of the Arrhenius equation:

$$R_{CO} = A \exp(-\frac{E_a}{RT})[FUEL] \quad (2)$$

where A is the frequency of successful collisions between reactant molecules that lead to reaction, E_a is the activation energy, i.e., the minimum energy required for the reaction to occur, R is the gas constant, and $[FUEL]$ is the fuel concentration.

Second, the calculation of temperature is based on the energy conservation equation, which is generally expressed as:

$$\rho c_p(\frac{\partial T}{\partial t} + u \cdot \nabla T) = \nabla \cdot (k \nabla T) + \dot{q} - \sum_i h_i \dot{m}_i \tag{3}$$

where ρ is the fluid density, c_p is the specific heat capacity at constant pressure, T is the temperature, k is the thermal conductivity, $\dot{q}$ is the volumetric heat source term, h_i is the enthalpy of the (i)-th chemical species, and $\dot{m}_i$ is the generation rate of the (i)-th chemical species.

In addition, smoke concentration is assessed by the light extinction coefficient k_c. A larger value of k_c indicates a higher smoke concentration and lower visibility. The relationship between visibility V and the light extinction coefficient k_c can be estimated using Koschmieder's law [35]. The calculation formula of k_c is as follows:

$$k_c = \frac{K}{V} \tag{4}$$

where V is the visibility, measured in meters, and K is a constant, usually taken as 3.912.

Fire is a dynamic process. During this process, once the real-time temperature, toxic gas concentration, or visibility reaches a high-risk level, the accessibility of evacuation nodes will be affected. Therefore, in order to further solve the dynamic route planning problem for passenger ship evacuation under fire spread conditions, it is necessary to define the hazard level of each node, dynamically update the hazard level of each node in the evacuation network during the evacuation process, and promptly eliminate impassable nodes and route segments.

Based on the above analysis of temperature, toxic gas concentration, and visibility in the evacuation network, after these parameters are calculated, the impact of fire on personnel evacuation is classified into three levels, namely safe, relatively dangerous, and highly dangerous, and the fire hazard level of each route node in the evacuation network is then determined [36]. Let P_i^t denote the safety status of node i at time t. Its calculation formula is given as follows:

$$P_i^t = \begin{cases} safe \quad node \begin{cases} 0 \le T < 30 \\ or \quad \rho_{co} < 0.1 \\ or \quad k_c < 0.4 \end{cases} \\ relatively \quad safe \quad node \begin{cases} 30 \le T < 60 \\ or \quad 0.1 \le \rho_{co} < 0.25 \\ or \quad 0.4 \le k_c < 1.2 \end{cases} \\ dangerous \quad node \begin{cases} 60 \le T < 120 \\ or \quad \rho_{co} \ge 0.25 \\ or \quad k_c \ge 1.2 \end{cases} \end{cases} \tag{5}$$

Specifically, when node i is in a safe state, $danger_i = 1$ is assigned, indicating that the fire hazard level of the route node is low and that node i is safe; under this condition, passengers can pass through normally. When node i is in a relatively safe state, $danger_i = 2$ is assigned, indicating that the fire hazard level of the route node is relatively high and that node i is in a relatively safe state; under this condition, passengers can barely pass through, and the evacuation route may be replanned according to the specific situation. When node i is a dangerous node, $danger_i = 3$ is assigned, indicating that the fire hazard level of the route node is extremely high and that node i is in a highly dangerous state. In this case, this study assumes that the fire has already spread to the node, making it unsuitable for

passenger passage, and evacuation routes with a higher safety level will be dynamically planned for evacuees.

In summary, the topological structure of the passenger ship fire emergency evacuation network constructed in this study is shown in Figure 4. The evacuation network, in addition to the basic route parameter information, such as d_{ij} and C_{ij}, which denote the distance and capacity of the route segment from node i to node j, respectively, also includes time-varying dynamic parameter information, such as $T_i(t)$, $\rho_i^{co}(t)$, $k_i^c(t)$, and $danger_i(t)$, which represent the temperature, CO concentration, light extinction coefficient, and fire hazard level at node i at time t, respectively.

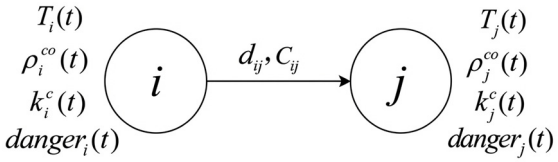


Figure 4. Emergency network evacuation topology diagram.

4. Construction of the Dynamic Route Planning Model for Passenger Ship Fire Emergency Evacuation

At present, originally passable routes inside passenger ships may reach hazardous states at certain times under the influence of multiple hazard sources, resulting in some routes becoming impassable and making route optimization a complex and challenging task. In addition, during evacuation, some studies directly ignore the impact of fire on passenger health and assume that passenger evacuation speed remains constant, which fails to accurately reflect real conditions. Therefore, to address the above issues, this study proposes a scientifically sound and reasonable dynamic route planning model for passenger ship fire emergency evacuation.

4.1. Problem Description and Model Assumptions

Once a fire occurs on a passenger ship, the evacuation environment continues to evolve with fire spread and smoke diffusion. As a result, routes that were originally passable may become hazardous or even invalid at a certain moment, making evacuation route selection highly dynamic and uncertain. Meanwhile, factors such as high temperature, smoke, changes in CO concentration, reduced visibility, and passenger panic continuously affect passengers' health conditions, mobility, and traffic efficiency, causing evacuation speed to exhibit clear time-varying characteristics. Therefore, traditional route planning methods that treat the evacuation environment as static and assume a constant movement speed are unable to accurately reflect the evacuation process under passenger ship fire conditions.

In addition, evacuation route planning for passenger ship fires is influenced not only by the dynamic changes in the fire environment, but also by multiple factors such as evacuation distance, evacuation time, and assembly station capacity. Excessive evacuation distance increases the exposure time of evacuees to hazardous conditions and aggravates the risk of corridor congestion. Evacuation time must satisfy the requirement that the required safe egress time be shorter than the available safe egress time. The limited capacity of assembly stations also imposes constraints on passenger allocation and route selection. Accordingly, passenger ship fire evacuation route planning is essentially a dynamic multi-objective optimization problem in a time-varying environment, where evacuation time, evacuation distance, and fire risk are jointly considered as optimization objectives, while constraints such as route feasibility, time safety, and capacity limits must also be satisfied. To this end, this paper develops a dynamic route planning model for passenger ship fire emergency evacuation to achieve a balance between evacuation efficiency and evacuation safety.

For the convenience of model solving, the following assumptions are made:

(1) The initial locations of evacuees, the number of evacuees, and the distances between nodes in the evacuation network are all known;

(2) The risk caused by the harm inflicted on passengers by emergency incidents is measurable;

(3) Emergency evacuation routes are determined based on the time-varying parameters of the evacuation network;

(4) Evacuees located at the same origin follow the same evacuation route and evacuate according to the designated guidance route until they reach the assigned exit, at which point the evacuation task is completed.

4.2. Construction of the Multi-Objective Dynamic Evacuation Route Planning Model for Passenger Ship Fires

In the dynamic evacuation route planning problem for passenger ships under fire conditions proposed in this study, multiple objectives need to be optimized. Multi-objective optimization theory aims to address optimization problems involving multiple conflicting objectives [37]. Therefore, this section establishes the objective functions and constraints of the multi-objective model developed in this study.

4.2.1. Multi-Objective Formulation of the Dynamic Evacuation Route Optimization Problem Under Time-Varying Conditions

In this study, factors such as fire spread, smoke diffusion, and crowd density in passenger ship fire evacuation are taken into account, and minimum evacuation time, minimum evacuation distance, and minimum fire risk are selected as the objective functions.

(1) Objective of Minimum Evacuation Time

$$\min f_1 = Minimize\left\{\sum_{i=s}^{n}\sum_{j=s}^{n} x_{ij}t_{ij}\right\} \tag{6}$$

This expression represents the minimization of evacuation time. During route planning, routes with shorter evacuation times are prioritized for evacuees to ensure that they can be evacuated to safe areas as quickly and safely as possible.

(2) Objective of Minimum Evacuation Distance

$$\min f_2 = Minimize\left\{\sum_{i=s}^{n}\sum_{j=s}^{n} x_{ij}d_{ij}\right\} \tag{7}$$

This expression represents the minimization of evacuation route distance. During route planning, routes with shorter evacuation distances are prioritized for evacuees to ensure that they can be evacuated to safe areas as quickly and safely as possible.

(3) Objective of Minimum Fire Risk

$$\min f_3 = Minimize\left\{\sum_{i=s}^{n}\sum_{j=s}^{n} x_{ij}r_{ij}\right\} \tag{8}$$

This expression represents the minimization of fire risk during evacuation. By taking the minimum fire risk level as the objective, the model dynamically plans available evacuation routes with higher safety, thereby improving evacuee safety throughout the evacuation process.

4.2.2. Construction of Constraints for the Dynamic Evacuation Route Optimization Problem Under Time-Varying Conditions

This study constructs the constraints by taking into account the dynamic properties of the fire environment from the perspectives of time, safety, feasibility, and resource limitations, so as to enhance the practical applicability of evacuation route optimization. The details are as follows:

(1) Time Constraint

In personnel evacuation under a ship fire scenario, the Euclidean distance between nodes i and j in the network graph can be expressed as follows:

$$d_{ij} = \sqrt{(x_j - x_i)^2 + (y_j - y_i)^2} \tag{9}$$

where d_{ij} is the Euclidean distance, measured in meters, x_i is the horizontal coordinate of node i, and y_i is its vertical coordinate.

The evacuation time of passengers on the passenger ship is calculated as follows:

$$t_{ij} = \frac{d_{ij}}{v_{ij}(t)} \tag{10}$$

The performance-based criterion for safe evacuation requires that the available safe egress time $ASET$ be greater than the required safe egress time $RSET$, i.e.,

$$ASET > RSET \tag{11}$$

(2) Route Feasibility Constraint

In constraint (12), x_{ij} is a decision variable that takes values of 0 or 1, where i = 1, 2, 3, . . ., d and j = 1, 2, . . ., d. Specifically, if a passageway e_{ij} is included in the evacuation route, then x_{ij} = 0, indicating the passageway can be used for evacuation. If the passageway e_{ij} is not included in the evacuation route, then x_{ij} = 1, indicating that this passageway cannot be used for evacuation.

$$x_{ij} = \begin{cases} 0, \text{passageway } e_{ij} \text{ belongs to the evacuation path} \\ 1, \text{passageway } e_{ij} \text{ not belongs to the evacuation path} \end{cases} \tag{12}$$

Constraint (13) ensures the feasibility of the route from the source node v_s to the exit v_d by restricting the value of x_{ij}.

$$\sum_{\substack{j=s \\ j \neq i}}^{n} x_{ij} - \sum_{\substack{j=s \\ j \neq i}}^{n} x_{ji} = \begin{cases} 1, i = s \\ -1, i = n \\ 0, otherwise \end{cases} \tag{13}$$

(3) Loop-Free Route Constraint

Constraint (14) is formulated to ensure, by restricting the value of node i, that the route from the source node to the exit node is unidirectional; that is, no route is allowed to return from the exit node to the source node, and no cyclic route is permitted.

$$\sum_{\substack{j=s \\ j \neq i}}^{n} x_{ij} \begin{cases} \leq 1, i \neq n \\ = -1, i = n \end{cases} \tag{14}$$

(4) Speed Constraint

In this study, the evacuation speed of evacuees in the absence of fire-related environmental influences is defined as v_{ij}^{w} based on the Weidmann model [38], which can be expressed as follows:

$$v_{ij}^{w} = v_0\left\{1 - \exp[-1.913(\frac{1}{\rho} - \frac{1}{\rho_{\max}})]\right\} \tag{15}$$

where v_0 is the free walking speed of passengers, ρ is the pedestrian density, $\rho = N_{ij}/s$, and $\rho_{\max}$ is the maximum pedestrian density (6 persons/m^2).

Under passenger ship fire conditions, evacuee movement speed decreases. Specifically, this reduction can be analyzed from the following aspects.

(1) CO

Liu et al. [39] quantified the extent to which different CO concentrations affect personnel evacuation. Based on this, the influence coefficient $f_1(\rho_{ij}^{co}(t))$ of the CO concentration on route (v_i, v_j) at time t (unit: (mg/m^3)) on evacuee movement speed is defined in this study as follows:

$$f_1(\rho_{ij}^{co}(t)) = \begin{cases} 1 & \rho_{ij}^{co}(t) < 0.1 \\ 1 - (0.2123 + 1.788\rho t_1) & 0.1 \le \rho_{ij}^{co}(t) < 0.25 \\ 0 & \rho_{ij}^{co}(t) \ge 0.25 \end{cases} \tag{16}$$

where t is the exposure time $t = t_j - t_i$, and t_i and t_j denote the times at which evacuees arrive at Nodes v_i and v_j, respectively, measured in seconds.

(2) Temperature

Different temperature levels have different degrees of influence on evacuation speed [40]. In this study, the influence coefficient $f_2(T_{ij}(t))$ of the temperature on evacuee movement speed on route (v_i, v_j) at time t is defined as follows:

$$f_2(T_{ij}(t)) = \begin{cases} 1 & T_0 \le T_{ij}(t) \le T_{e1} \\ \frac{(v_{\max} - 1.2)(\frac{T_{ij}(t) - T_{e1}}{T_{e2} - T_{e1}})^2}{v_0} + 1 & T_{e1} \le T_{ij}(t) \le T_{e2} \\ \frac{v_{\max}}{1.2}\left[1 - (\frac{T_{ij}(t) - T_{e2}}{T_d - T_{e2}})^2\right] & T_{e2} \le T_{ij}(t) \le T_d \end{cases} \tag{17}$$

where $T_{ij}(t)$ is the actual temperature (in °C) experienced by evacuees while moving along arc (v_i, v_j); T_0 is the room temperature (set to 20 °C); v_0 is the normal walking speed (set to 1 m/s); $v_{\max}$ is the maximum walking speed (set to 5 m/s); T_{e1} is the temperature that causes discomfort (set to 30 °C); T_{e2} is the temperature that causes injury (set to 60 °C); and T_d is the lethal temperature (set to 120 °C). When the temperature exceeds 120 °C, $f_2(T_{ij}(t))$ is equal to 0.

(3) Visibility

In this study, the influence coefficient $f_3(k_{ij}^{c}(t))$ of visibility on evacuee movement speed on route (v_i, v_j) at time t is defined as follows:

$$f_3(k_{ij}^{c}(t)) = \begin{cases} 1, & k_{ij}^{c}(t) \le 0.4 \\ 1.375 - 0.9375K_{ij}^{c}(t), & 0.4 < k_{ij}^{c}(t) \le 1.2 \\ 0.25 & k_{ij}^{c}(t) > 1.2 \end{cases} \tag{18}$$

The fire scenario index is defined as follows:

$$W_{ij}(t) = f_1(\rho_{ij}^{co}(t)) \times f_2(T_{ij}(t)) \times f_3(k_{ij}^{c}(t)) \tag{19}$$

(4) Crowd Density

The crowd density $\rho_{ij}(t)$ on route (v_i, v_j) at time t is defined in this study as follows:

$$\rho_{ij}(t) = \frac{q_{ij}}{C_{ij}} \tag{20}$$

where q_{ij} denotes the number of evacuees in the passageway, and C_{ij} denotes the passage capacity, i.e., the maximum number of evacuees that the passageway can accommodate under ideal conditions. In general, a passageway is assumed to accommodate no more than 6 persons per square meter. Once this value is exceeded, the passageway tends to become excessively crowded, thereby hindering pedestrian movement.

The congestion coefficient $k_\rho(t)$ on route (v_i, v_j) at time t is defined as follows:

$$k_\rho(t) = \begin{cases} 1, & \rho_{ij}(t) < 0.5. \\ e^{\alpha(\frac{q_{ij}}{C_{ij}})-0.5}, & 0.5 \le \rho_{ij}(t) \le 1 \\ e^{\alpha(\frac{q_{ij}}{C_{ij}})-0.5} - 10^5 \times (\frac{q_{ij}}{C_{ij}} - 1), & \rho_{ij}(t) > 1 \end{cases} \tag{21}$$

where $\forall i, j \in S_0 \cup S_1$ and α is the congestion correction coefficient, which is generally set to 0.5; in passenger ship evacuation route planning, the traffic capacity of a passageway must be taken into account, and the number of evacuees waiting in the passageway should be limited to its admissible capacity, i.e., $q_{ij} \le C_{ij}$. Meanwhile, a congestion penalty factor is introduced into the formula for the congestion coefficient to reflect that passengers tend to choose alternative routes with better traffic conditions when facing severely congested routes.

Accordingly, the speed $v_{ij}(t)$ of a person moving along route (v_i, v_j) in a passenger ship fire scenario can be expressed as follows:

$$v_{ij}(t) = v_{ij}^w \times W_{ij}(t) \times k_\rho(t) \tag{22}$$

(5) Assembly Station Capacity Constraint

When determining the optimal passenger ship evacuation route while considering assembly station capacity, the constraints are formulated as follows:

$$\sum_{j=1}^{m} a_{ij} = p_i \tag{23}$$

$$\sum_{i=1}^{n} a_{ij} \le C_j \tag{24}$$

$$a_{ij} \ge 0 \tag{25}$$

Constraint (23) indicates that all evacuees at each node i must be fully assigned to the m exits. Constraint (24) indicates that the total number of evacuees assigned to each exit j must not exceed its capacity C_j. Constraint (25) indicates that the number of evacuees assigned from each node to each exit must be a non-negative integer.

4.3. Improved Ant Colony Optimization for Solving the Multi-Objective Dynamic Evacuation Route Optimization Model

The passenger ship fire evacuation route planning problem considered in this study is a discrete, graph-based, dynamic multi-objective optimization problem. The evacuation route is composed of a sequence of interconnected nodes and edges, while the edge costs and node accessibility vary over time due to fire spread, smoke diffusion, temperature rise,

visibility reduction, changes in CO concentration, congestion level, and passage availability. Therefore, the solution method should be able to construct feasible paths directly on the evacuation network, incorporate time-varying environmental information into the route selection process, and maintain a balance between exploration and exploitation under multiple conflicting objectives.

Compared with other available metaheuristic algorithms, such as genetic algorithms (GAs), particle swarm optimization (PSO), artificial immune systems (AISs), simulated annealing (SA), differential evolution (DE), and fruit fly optimization algorithm (FOA), ant colony optimization (ACO) has several computational and operational advantages for the specific dynamic route planning problem considered in this study. Firstly, ACO is inherently suitable for discrete network path planning because ants construct routes step by step according to the connectivity of the graph, which is consistent with the node-by-node decision-making process of evacuation route selection. In contrast, GA usually requires chromosome encoding and decoding schemes to represent paths, and crossover or mutation operations may generate infeasible, disconnected, or cyclic routes. PSO and DE were originally designed for continuous optimization problems and therefore have certain limitations when dealing with discrete network-node-based route planning problems. AIS and SA can also be applied to combinatorial optimization problems. However, when they are used for graph-based path planning, their neighborhood generation or solution perturbation operations may also produce infeasible, disconnected, or cyclic routes. In addition, the search mechanism of FOA mainly relies on random search and local optimization, which may lead to a rapid increase in computational time in complex scenarios.

Secondly, the pheromone mechanism of ACO provides a distributed memory of high-quality route segments. Through pheromone evaporation and reinforcement, the search process can gradually weaken outdated or unsafe routes and strengthen route segments with better performance under the current fire conditions. This feature is particularly suitable for evacuation environments in which route safety, travel time, congestion level, and node accessibility change dynamically with fire spread. Thirdly, the heuristic information in ACO can be flexibly redesigned to incorporate evacuation distance, evacuation time, fire risk, congestion, and environmental conditions, making it suitable for the multi-objective optimization structure of this study. Finally, the population-based search process of ACO can generate multiple candidate routes in one iteration, which facilitates the identification of Pareto solutions and further supports evacuation route selection under muster station capacity constraints.

Therefore, this section improves the ant colony algorithm and proposes a solution algorithm for the dynamic evacuation route multi-objective optimization model based on the improved ant colony algorithm. The improvements include: (1) applying linear interpolation to fire environment parameters, such as carbon monoxide concentration, temperature, and visibility, to accurately estimate conditions at each evacuation node at any time; (2) designing a heuristic function that jointly considers multiple evacuation objectives; (3) introducing a non-dominated sorting-based multi-objective pheromone update mechanism to identify routes with better overall performance; and (4) adopting an adaptive backtracking strategy to prevent the algorithm from entering dead loops.

4.3.1. Workflow of the Improved Ant Colony Optimization Algorithm

The flowchart of the improved ACO algorithm is shown in Figure 5.

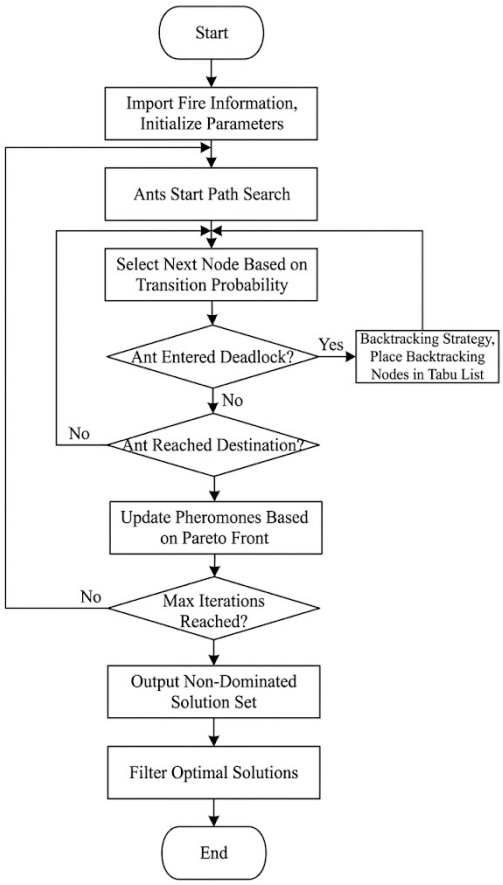


Figure 5. Algorithm flow chart.

In the step of filtering the optimal solution, the weighted ideal point method is employed in this study to screen the Pareto solutions and determine the final evacuation route. The corresponding formula of the weighted ideal point method is given as follows:

$$\min F = r_1 \frac{f_1 - {f_1}^*}{{f_1}^*} + \ldots + r_n \frac{f_n - {f_n}^*}{{f_n}^*} \tag{26}$$

where $\vec{f} = ({f_1}^*, \ldots, {f_n}^*)$ denotes the ideal point, $\vec{r} \in R = \left\{ \vec{r} \middle| r_i \geq 0, \sum r_i = 1, i = 1, \ldots n \right\}$ is the weight coefficient vector, and (n = 3), corresponding to the three objectives, namely evacuation time, evacuation distance, and fire risk. F represents the total cost of the three optimization objectives from each source node to the destination node.

4.3.2. Parameter Processing

To fill data gaps and generate new data points, this study adopts the linear interpolation method for estimation. Linear interpolation is a commonly used approach that estimates the value of an unknown point by connecting known data points. Specifically, the formula of the interpolation function is as follows:

$$f(t) = \frac{(t - t_1)}{(t_2 - t_1)} \cdot (y_2 - y_1) + y_1 \tag{27}$$

where t is the interpolation time point, t_1 and t_2 are known time points, and y_1 and y_2 are the corresponding parameter values.

The interpolated values of carbon monoxide concentration, temperature, and visibility are used to calculate the fire environmental parameters for each route, and these parameters are further used to characterize the extent to which fire affects evacuees' movement speed.

4.3.3. Construction of the Heuristic Function

In the passenger ship fire evacuation route planning problem considered in this study, the optimal route depends not only on distance, but also on factors such as time, risk, congestion, and environmental conditions. The traditional heuristic function tends to guide ants toward the shortest route while ignoring high-risk areas along that route, which may lead to an overall solution that is not sufficiently reasonable. Therefore, considering the effects of evacuation distance, evacuation time, and fire environmental factors on evacuees, this study defines a comprehensive heuristic function as follows.

$$\eta_{ij} = \frac{1}{w_1 d_{ij} + w_2 t_{ij} + w_3 r_{ij}} \tag{28}$$

where w_1, w_2, and w_3 are the weight coefficients corresponding to the respective evacuation objectives. The weight coefficients are determined using the expert scoring method.

4.3.4. Pheromone Update Rule Design

This study involves a multi-objective path planning problem, for which the classical single-objective path quality evaluation method is no longer applicable. Therefore, this study proposes an improved pheromone update strategy by incorporating a non-dominated sorting mechanism into the traditional pheromone update rule. Specifically, the solutions that are not dominated by any other solution in all objectives are identified to form the Pareto front, and pheromones are then updated based on these solutions. In this way, high-quality non-dominated solutions can exert a stronger guiding effect on route search, thereby avoiding entrapment in local optima and improving the quality of route planning results. The specific update rules are as follows:

(1) Pheromone Evaporation

Pheromone evaporation refers to the gradual decrease in pheromone concentration on a route over time, simulating the natural evaporation of pheromones in the real world. Its mathematical expression is given as follows:

$$\tau_{ij}(t+1) = (1-\rho)\cdot\tau_{ij}(t) \tag{29}$$

where $\tau_{ij}(t)$ denotes the pheromone concentration on (i, j) at time t, and $\rho \in [0, 1]$ is the pheromone evaporation coefficient, which controls the evaporation rate of pheromone. The larger its value, the faster the pheromone evaporates.

(2) Pheromone Reinforcement

To allow non-dominated solutions to exert a greater influence on pheromone updating, this study adopts a pheromone update method based on Pareto front ranks:

$$\Delta\tau_{ij}(t) = \begin{cases} \frac{Q}{L_k}\cdot\alpha^r, & P_k \; belongs \;\; to \;\; the \;\; r\text{-}th \;\; Pareto \;\; front \\ 0, & otherwise \end{cases} \tag{30}$$

where α denotes the front attenuation coefficient, $\alpha \in (0, 1]$, and r represents the Pareto front rank to which solution P_k belongs. Better-ranked fronts are assigned larger weights; that is, solutions on the first front exert the greatest influence, while the influence of solutions on subsequent fronts decreases progressively.

4.3.5. Improved Deadlock Handling Strategy

To address this issue, this study proposes three main improvement mechanisms. (1) State transition constraints. When selecting the next node, if a node has already been visited in the current route, it is prohibited from being selected unless no other candidate nodes are available. In this way, repeated cycling between the same nodes is avoided.

(2) Adaptive route backtracking strategy. When an ant encounters a situation in which no neighboring node is available for selection, that is, all neighboring nodes have already been visited, it is allowed to backtrack to the previous node and reselect the route. This strategy not only prevents dead loops but also increases the flexibility of route searching. (3) Random exploration mechanism. When all neighboring nodes have been visited, the ant is allowed, with a certain probability, to randomly select an unvisited node for exploration, thereby increasing search diversity.

To describe this mechanism, let the current node be i, its neighboring node set be $N(i)$, the set of visited nodes be T, and the node selected in the next step be j. The selection probability of node j can be expressed as follows:

$$P_{ij} = \begin{cases} \frac{\tau_{ij}^{\alpha} \cdot \eta_{ij}^{\beta}}{\sum_{k \in N(i) \setminus T} \tau_{ij}^{\alpha} \cdot \eta_{ik}^{\beta}} & j \notin T \\ 0, & j \in T \end{cases} \tag{31}$$

where τ_{ij} denotes the pheromone concentration, η_{ij} denotes the heuristic information, α and β are the parameters controlling the influence of pheromone and heuristic information on the selection probability, respectively, and T is the set of visited nodes. When all neighboring nodes have already been visited, the ant must either backtrack or randomly select a new node.

5. Simulation Experiments

In this section, simulation experiments and comparative experiments are conducted based on the publicly available ship evacuation dataset from the SAFEGUARD project under the European Union's Seventh Framework Program (FP7), in order to validate the effectiveness and practical applicability of the dynamic route planning model for passenger ship fire emergency evacuation proposed in this study, as well as the corresponding solution algorithm.

5.1. Evacuation Network Construction

5.1.1. Dataset Description

The SAFEGUARD project under the European Union's Seventh Framework Program [41] was funded by the European Union and provides comprehensive data for the calibration and validation of ship-based evacuation models. By investigating and analyzing different benchmark scenarios, the project provides full-scale data and computer-aided design (CAD) drawings for three different types of ships. Five full-scale evacuation experiments were conducted on three different vessels, during which important data related to onboard human behavior, ship characteristics, evacuation route planning, ship design, and safety operations were collected, with the aim of improving passenger safety on board. The project is characterized by a high scientific standard and rigorous research procedures.

The dataset of the first ship (RP1) is complete, and has a typical structure and moderate complexity, which is convenient for constructing the evacuation network. Therefore, the CAD data of the lower deck of the first ship (RP1) are selected to construct the evacuation network, which serves as the basis for the subsequent study of personnel evacuation route planning under ship fire scenarios, as shown in Figure 6. The figure illustrates the layout of the first deck of the cruise ship operated by Color Line, which can accommodate approximately 1300 passengers and crew members. The deck is approximately 150 m long, 28 m wide, and 3 m high, and includes passenger spaces, large retail and restaurant/dining areas, bar areas, and muster station C.

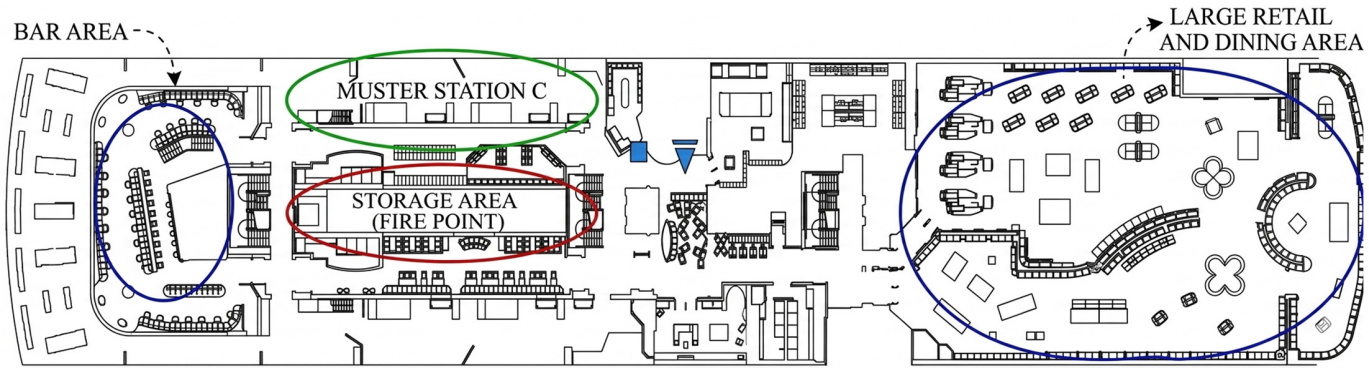


Figure 6. CAD drawing of the bottom deck.

5.1.2. Network Representation of the Evacuation Environment

According to the ship dataset under study and the definition of the emergency evacuation network topology, the emergency evacuation network topology of the first deck can be constructed as shown in Figure 7. This topology is formed by connecting the centroids of different areas. The network consists of 23 nodes and 30 edges, where the edges represent the passageways within the ship, and the nodes represent the intersections of these passageways. Since fire-prone areas are generally located in storage areas, and the storage area corresponds to Node 7, Node 7 is designated as the fire node in this study. In addition, Node 15 and Node 23 are connected to the assembly area, and these two locations are therefore designated as exit nodes.

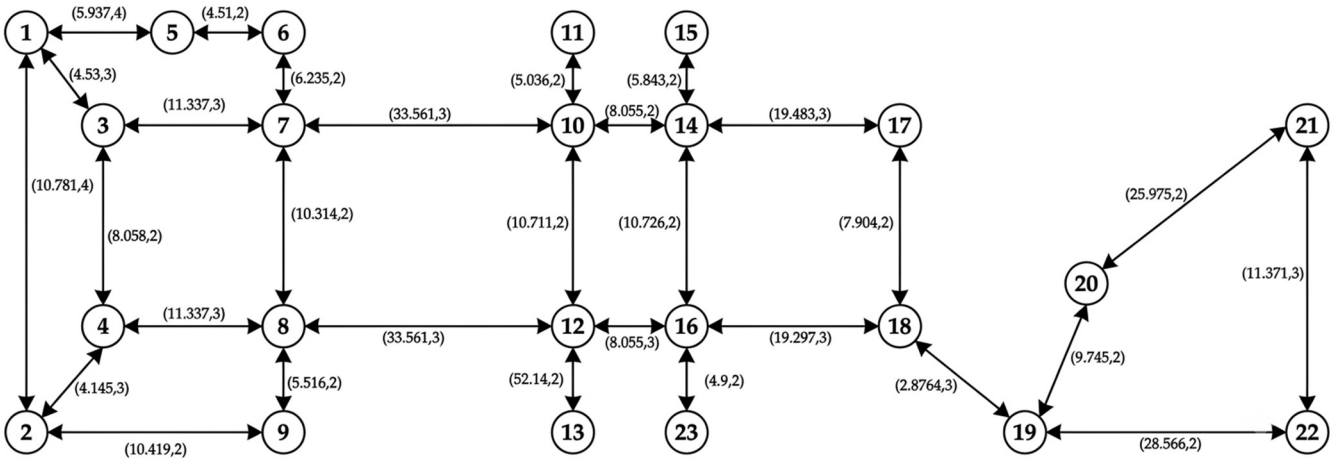


Figure 7. Emergency evacuation network topology diagram.

The coordinates of each node in the emergency evacuation network topology are listed in Table 1.

Table 1. Coordinate information of network nodes.

Node ID	Coordinate	Node ID	Coordinate
1	(0.413, 10.841)	13	(48.715, −4.824)
2	(0, 0)	14	(56.86, 11.377)
3	(4.441, 8.648)	15	(56.86, 17.15)
4	(4.109, 0.622)	16	(56.86, 0.413)
5	(5.153, 13.906)	17	(76.328, 8.647)
6	(9.718, 13.862)	18	(76.373, 0.636)
7	(15.153, 10.997)	19	(104.814, 1.507)

Table 1. *Cont.*

Node ID	Coordinate	Node ID	Coordinate
8	(15.153, 0.57)	20	(107.365, 11.084)
9	(10.255, −1.936)	21	(133.501, 11.173)
10	(48.805, 11.377)	22	(133.456, −0.552)
11	(48.76, 16.434)	23	(56.809, −4.379)
12	(48.626, 0.368)		

5.1.3. Calculation of Evacuation Network Parameters

Based on fire dynamics theory, the fire spread model was developed using PyroSim, and a three-dimensional ship model was established. The resulting fire simulation model is shown in Figure 8.

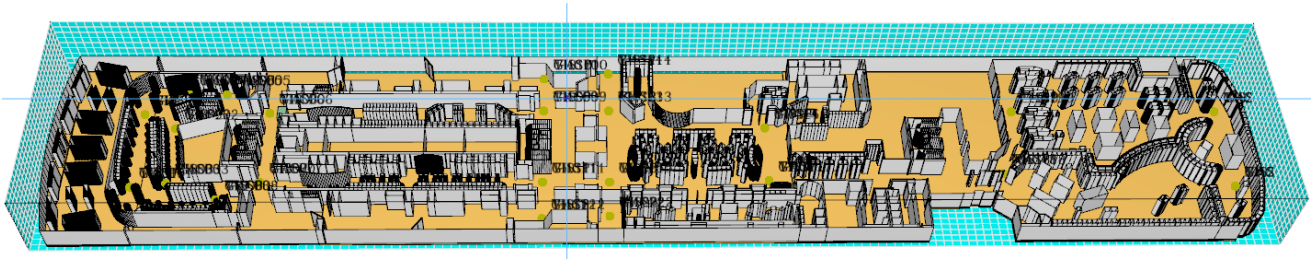


Figure 8. Fire simulation model of the bottom deck.

The initial simulation conditions were then specified. In this study, detectors for CO concentration, temperature, and visibility were installed at each evacuation node in the network topology. These detectors were placed at a height of 1.8 m above the ground, and the initial temperature was set to 20 °C. Meanwhile, a storage area with excessive accumulated miscellaneous materials was selected as the ignition location, and a fire source was assigned to this area with a fire source area of 2.54 m^2.

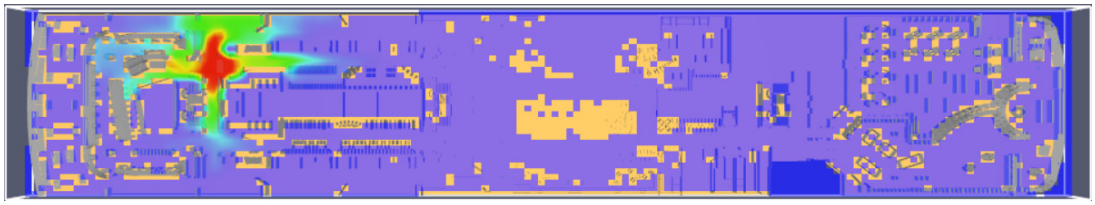
When setting the heat release rate for the passenger ship fire, the standardized provisions for the maximum heat release rate in the Code for Smoke Control and Exhaust of Buildings, as presented in Table 2, were taken as a reference. Considering that passenger ship cabins are enclosed spaces with poor ventilation and limited exits, and that these characteristics are, to some extent, similar to those of garages and warehouses, this study assumes that the ship's sprinkler system operates effectively and that the fire source burns within a limited range. Accordingly, the heat release rate adopted for this passenger ship fire simulation was finally determined to be 2000 kW.

Table 2. Maximum heat release rate standard.

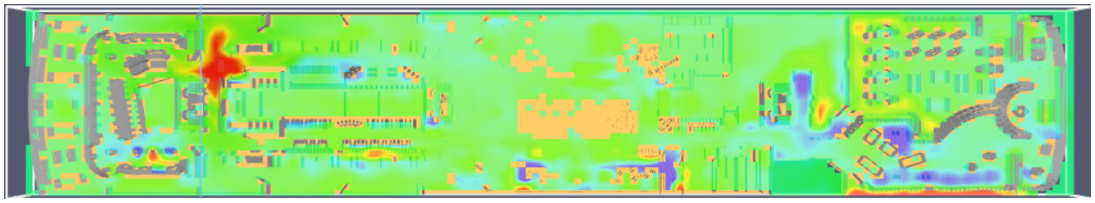
Building Type	Maximum Heat Release Rate Q/KW	
	With Sprinklers	Without Sprinklers
Shopping mall	2000	-
Office, Guest room	1500	6000
Public place	2500	8000
Garage	2500	20,000
Supermarket, Warehouse	4000	20,000

After running the FDS fire spread model, the changes in CO concentration, temperature, and visibility at different locations of the passenger ship can be obtained from the Smokeview visualization. By examining the slices of CO concentration, temperature, and

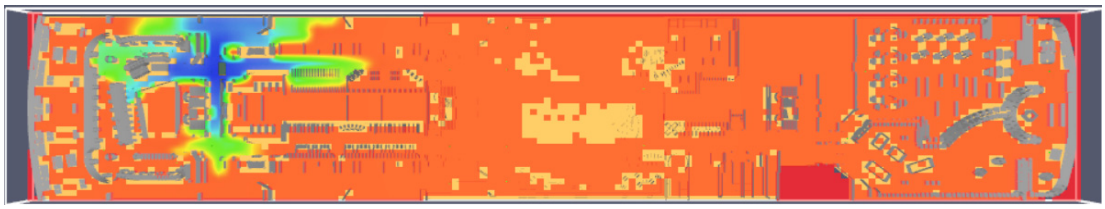
visibility, the fire conditions at different time points can be observed clearly and intuitively. Figure 9 presents an example of the fire state at 120 s of combustion as displayed in the Smokeview animation. As the fire develops, smoke gradually spreads to other areas of the passenger ship, resulting in a progressive decrease in visibility throughout the ship, while temperature and CO concentration gradually increase. In Figure 9a, the red regions generally indicate higher CO concentrations, while the purple regions indicate lower CO concentrations. In Figure 9b, the red regions represent higher temperatures, whereas the green regions represent lower temperatures. In Figure 9c, the orange regions indicate higher visibility, while the green and blue regions indicate lower visibility.



(**a**) CO concentration



(**b**) Temperature



(**c**) Visibility

Figure 9. Sectional diagram of flue gas diffusion, CO concentration, temperature, and visibility at t = 120 s.

After completing the passenger ship fire simulation in PyroSim 2023.3.1312, the CO concentration detectors, temperature detectors, and visibility detectors installed at each node can provide the fire-related data at different nodes and at different time points. These data are then used as the basis for calculating the fire risk level along evacuation routes in this study, and provide data support for the improved ant colony optimization algorithm. Tables 3–5 present the fire risk values of each path at different burning times of t = 30 s, t = 120 s, and t = 300 s, respectively.

Table 3. The fire risk values of each path when the burning time t = 30 s.

Route	CO Concentration	Temperature	Visibility	Route	CO Concentration	Temperature	Visibility
v1–v2	0	20.038	30	v10–v12	0	21.336	30
v1–v3	1.305	17.097	30	v10–v14	0	20.006	30
v1–v5	5.841	20.590	30	v12–v13	0	18.758	30
v2–v4	0	17.816	30	v12–v16	0	21.715	30
v2–v9	0	19.345	30	v14–v15	0	19.984	30
v3–v4	1.304	14.875	30	v14–v16	0	20.384	30

Table 3. *Cont.*

Route	CO Concentration	Temperature	Visibility	Route	CO Concentration	Temperature	Visibility
v3–v7	79.674	24.560	16.989	v14–v17	0	20.663	30
v4–v8	8.078	17.121	30	v16–v18	0	23.894	30
v5–v6	39.109	24.581	19.574	v16–v23	0	22.505	30
v6–v7	111.637	31.545	6.561	v17–v18	0	24.173	30
v7–v8	86.448	26.805	16.989	v18–v19	0	23.510	30
v7–v10	78.369	27.514	16.989	v19–v20	0	18.720	30
v8–v9	8.078	18.651	30	v19–v22	0	20	30
v8–v12	8.078	19.304	30	v20–v21	0	22.216	30
v10–v11	0	20.064	30	v21–v22	0	23.497	30

Table 4. The fire risk values of each path when the burning time t = 120 s.

Route	CO Concentration	Temperature	Visibility	Route	CO Concentration	Temperature	Visibility
v1–v2	22.237	19.525	22.401	v10–v12	0	21.212	30
v1–v3	67.322	25.086	10.625	v10–v14	0	19.760	30
v1–v5	52.670	22.625	12.003	v12–v13	0	22.136	30
v2–v4	6.675	15.515	30	v12–v16	0	21.802	30
v2–v9	2.139	22.247	30	v14–v15	0	19.853	30
v3–v4	51.760	22.275	18.224	v14–v16	0	20.350	30
v3–v7	254.066	40.475	4.021	v14–v17	0	18.908	30
v4–v8	24.538	19.294	22.542	v16–v18	0	21.329	30
v5–v6	79.454	23.477	7.806	v16–v23	0	21.169	30
v6–v7	253.932	38.979	4.003	v17–v18	0	19.887	30
v7–v8	226.845	38.693	8.339	v18–v19	0	20.715	30
v7–v10	206.947	36.766	15.797	v19–v20	0	27.676	30
v8–v9	20.001	26.027	22.542	v19–v22	0	20	30
v8–v12	19.898	23.125	22.542	v20–v21	0	27.676	30
v10–v11	0	18.544	30	v21–v22	0	19.060	30

Table 5. The fire risk values of each path when the burning time t = 300 s.

Route	CO Concentration	Temperature	Visibility	Route	CO Concentration	Temperature	Visibility
v1–v2	155.248	26.764	5.639	v10–v12	8.748	18.602	30
v1–v3	249.148	31.085	2.470	v10–v14	11.198	16.822	30
v1–v5	284.308	39.852	2.270	v12–v13	0.889	20.696	30
v2–v4	64.892	14.312	8.960	v12–v16	0.545	19.927	30
v2–v9	53.732	27.064	12.144	v14–v15	3.632	17.694	30
v3–v4	158.791	18.633	5.791	v14–v16	2.995	18.147	30
v3–v7	328.188	35.786	1.985	v14–v17	3.198	13.871	30
v4–v8	56.041	16.838	10.626	v16–v18	0	16.955	30
v5–v6	355.008	43.211	1.813	v16–v23	0	21.601	30
v6–v7	393.214	46.385	1.644	v17–v18	0.291	12.678	30
v7–v8	225.438	33.992	6.820	v18–v19	0	16.798	30
v7–v10	209.033	32.695	15.807	v19–v20	0	30.438	30
v8–v9	44.881	29.591	13.810	v19–v22	0	20	30
v8–v12	25.152	19.899	21.013	v20–v21	0	30.438	30
v10–v11	19.521	16.661	27.953	v21–v22	0	18.443	30

Meanwhile, based on the data obtained from the fire simulation and the definitions of risk thresholds for the fire-related parameters established in this study, the corresponding times t_i^1 and t_i^2 at which the safety state of each node changes can be determined, as shown in Table 6. Here, t_i^1 denotes the time at which node i changes from a safe state to a barely passable state; t_i^2 denotes the time at which node i changes from a barely passable state to a hardly passable state; and None indicates that node i remains in a safe state throughout the entire process.

Table 6. The change of node security status corresponds to the timetable.

Node ID	t_i^1	t_i^2	Node ID	t_i^1	t_i^2
1	132.384	None	13	None	None
2	None	None	14	None	None
3	62.539	95.563	15	101.177	None
4	None	None	16	None	None
5	53.783	102.365	17	178.202	None
6	42.649	106.505	18	None	None
7	28.438	36.626	19	None	None
8	207.094	None	20	None	None
9	241.527	None	21	None	None
10	None	None	22	None	None
11	None	None	23	None	None
12	None	None			

The fire simulation data were obtained by detecting the fire-related parameters at each node in the network topology, and the real-time hazard level of each node was then determined according to changes in the risk index, as shown in Figure 10. This figure presents the network topology at 300 s after the fire outbreak, indicating the status of each node when the fire has burned for 300 s. Green nodes represent that stay in a safe state, such as Node 10 and Node 11; blue nodes represent that stay in a relatively hazardous state, such as Node 1 and Node 8; and red nodes represent that stay in a dangerous state, such as Node 6 and Node 7. Under such conditions, evacuees must urgently avoid these dangerous nodes during the evacuation process to ensure personal safety.

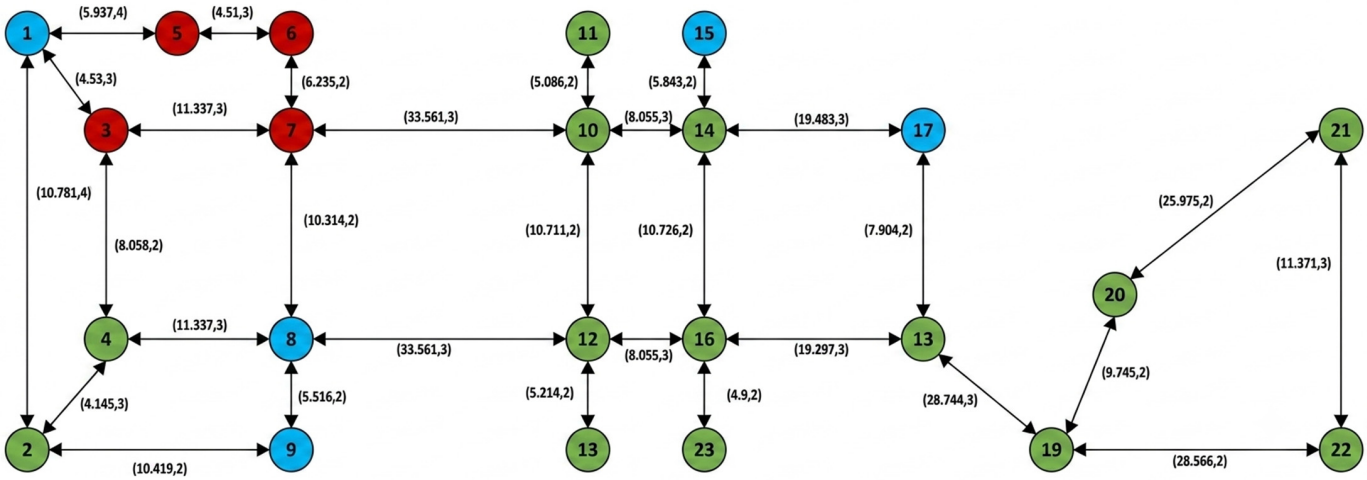
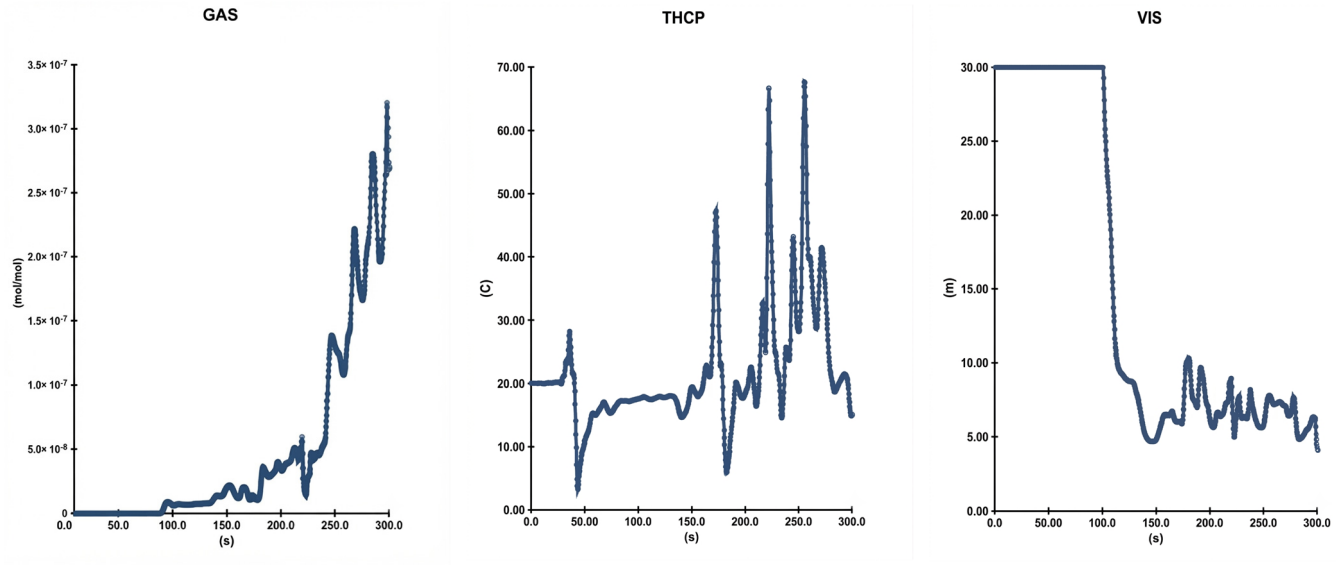


Figure 10. The topology diagram when the burning time t = 300 s.

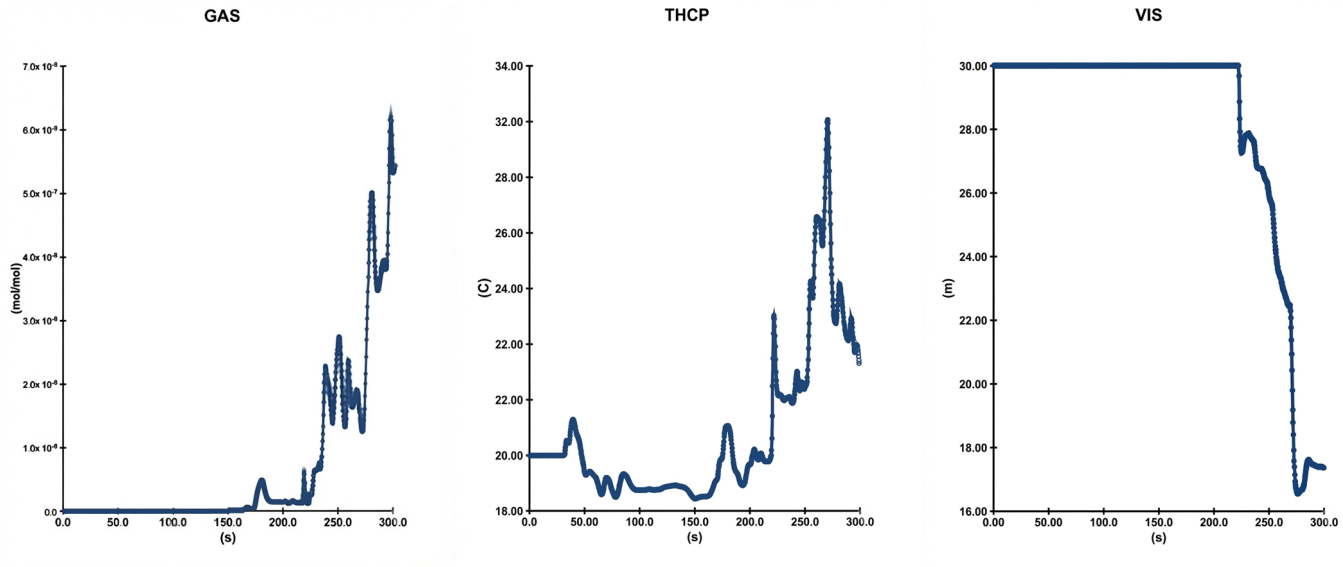
Under fire conditions, as time progresses, the fire risk levels at the nodes in the evacuation network generally show an increasing trend. In this case, Node 15 and Node 23 are designated as safety exits. Taking these two safety exits as examples, this study

analyzes their fire conditions. Figures 11 and 12 present the line charts of the fire-related data at exit Node 15 and exit Node 23 over time, respectively. From left to right, the plots show the variations in CO concentration, temperature, and visibility.



(**a**) CO concentration (**b**) Temperature (**c**) Visibility

Figure 11. Line chart of fire data change over time at exit Node 15.



(**a**) CO concentration (**b**) Temperature (**c**) Visibility

Figure 12. Manner line chart of fire data change over time at exit Node 23.

The data of the exit nodes obtained from the PyroSim fire simulation show that CO concentration and temperature exhibit a fluctuating upward trend, whereas visibility shows a fluctuating downward trend. Since exit Node 15 is relatively far from the ignition node, none of these parameters changes significantly within the first 100 s after the fire starts, and the exit node therefore remains in a relatively safe state during this short period. When the fire has burned for about 100 s, the fire-related data at the exit begin to change noticeably. By approximately 250–300 s after ignition, the fire risk factors at the exit have basically reached the predefined threshold for dangerous nodes. Therefore, emergency evacuation should be carried out efficiently, and high-risk nodes and routes should be avoided as the

fire develops, so as to prevent casualties caused by evacuees remaining at the fire scene for an extended period.

Meanwhile, compared with exit Node 15, exit Node 23 is farther from the ignition node and therefore remains in a safe state for a longer period. In the early stage of the fire, the fire-related parameters at Node 23 show no obvious changes. It is not until the fire has burned for about 160 s that CO concentration and temperature begin to exhibit a noticeable upward trend. Visibility does not begin to decline until approximately 200 s after the fire breaks out. These results indicate that, in a multi-exit evacuation scenario after a fire, the safety status of each exit continues to change over time. Therefore, during the evacuation process, it is essential to select more appropriate exits for evacuees and to plan reasonable and scientifically sound evacuation routes, which are of great practical significance.

5.2. Personnel Evacuation Simulation

This section mainly applies the proposed model to a fire evacuation simulation scenario on the first deck of the RP1 ship for testing. The numerical variations in the three risk factors, namely CO concentration, temperature, and visibility, can be obtained from the fire simulation analysis in the previous section. After these data are imported into the route planning model based on the improved ant colony optimization algorithm, the model parameters are set, and the personnel evacuation simulation is then carried out to reproduce the evacuation process, ultimately yielding the optimal evacuation routes.

5.2.1. Parameter Settings

The dynamic route planning model and the improved ACO algorithm were implemented and solved in MATLABR 2024a. The simulation parameters in this study were set by referring to commonly used values in ant colony optimization algorithms and related studies on path planning and multi-objective optimization, and were adjusted according to the characteristics of the problem addressed in this study. The number of ants m was set to 5, the maximum number of iterations was set to 30, the pheromone importance factor was set to 1, the heuristic factor was set to 2, the pheromone evaporation coefficient was set to 0.1, the pheromone reinforcement intensity was set to 100, and the weights of distance, time, and fire risk were set to 0.3, 0.6, and 0.1, respectively.

According to the relevant literature, the relationships of walking speed with gender, age, and body mass among the Chinese population are shown in Table 7.

Table 7. Comparison Table of Characteristics of Emergency Evacuation Personnel and Evacuation Speed.

No. (Feature)	Gender	Age (Years)	Height/m	Mass/kg	Speed/($m \cdot s^{-1}$)
1	male	20~30	1.7	60	1.5
2	female	20~30	1.6	52	1.35
3	male	31~40	1.7	60	1.35
4	female	31~40	1.6	52	1.22
5	male	41~50	1.69	60.5	1.22
6	female	41~50	1.59	52.5	1.10
7	male	51~60	1.68	61	1.10
8	female	51~60	1.58	53	1.00

To ensure that evacuees can avoid the fire and be evacuated successfully, a female with a height of 1.58 m and an age between 51 and 60 years, as listed in the table, is taken as the reference, and the corresponding walking speed is set to 1 m/s.

In addition, it is assumed that the capacities of the two exits are both 165 persons, and that the total number of evacuees is 305. According to the daytime population distribution in different areas of the ship, the number of evacuees at each node is set as shown in Table 8.

Table 8. Number of evacuees at each node.

Node ID	Number of People	Node ID	Number of People
1	12	13	14
2	10	14	28
3	8	15	0
4	8	16	2
5	6	17	8
6	4	18	24
7	1	19	7
8	8	20	52
9	12	21	29
10	6	22	24
11	14	23	0
12	28		

5.2.2. Experimental Results

Considering that assembly station capacity is limited, evacuees at each node must first be assigned to specific exits before the total evacuation cost can be calculated. Therefore, this study first plans the optimal evacuation route for the evacuees at each node toward different exits based on the proposed dynamic route planning model for passenger ship emergency evacuation and the improved ant colony optimization algorithm, thereby obtaining the Pareto fronts from each node to each exit. Taking Node 1 as an example, the Pareto front distributions of evacuation routes from this node to Exit 1 (Node 15) and Exit 2 (Node 23), considering the three optimization objectives of evacuation time, evacuation distance, and fire risk, are shown in Figures 13a and 13b, respectively. Each point in the three-dimensional space represents a feasible evacuation route.

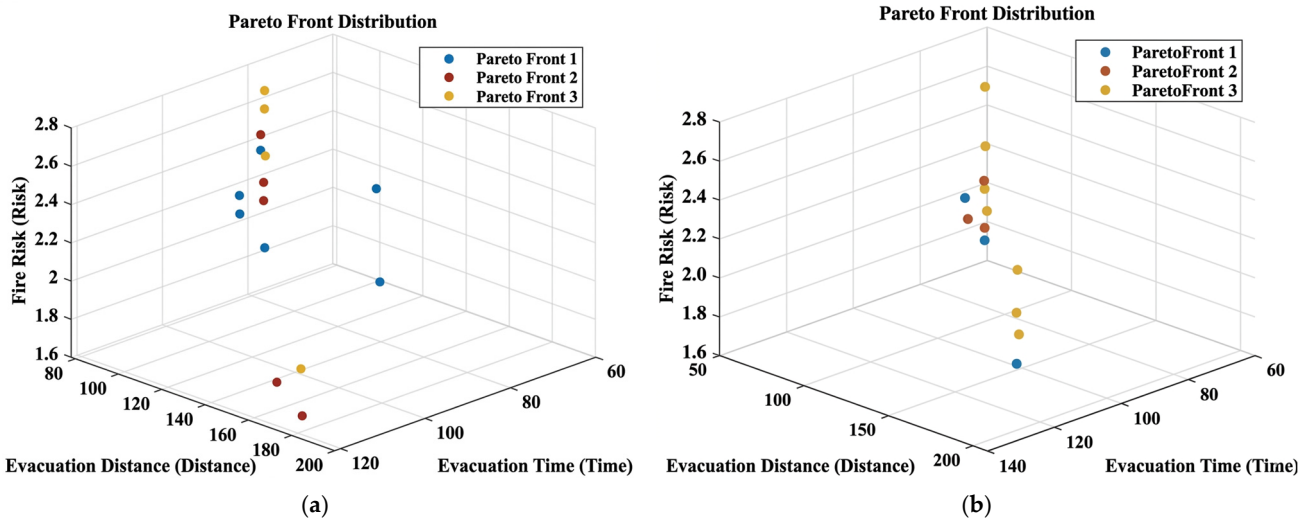


Figure 13. Pareto frontier distribution. (**a**) Pareto frontier distribution from Node 1 to Exit 1. (**b**) Pareto frontier distribution from Node 1 to Exit 2.

Since all three objectives in this study are minimization objectives, smaller values of evacuation time, evacuation distance, and fire risk indicate better overall performance of the route scheme. The points with different colors in the figure represent different

levels of Pareto fronts. The blue points represent the first Pareto front, which consists of non-dominated solutions. This means that no other route can outperform these solutions simultaneously in all three objectives, reflecting the optimal trade-off among evacuation efficiency, route length, and fire safety. In contrast, the second- and third-level Pareto solutions, represented by orange and yellow points, do not exhibit such an optimal trade-off. For example, some routes may have shorter evacuation times but pass through areas with higher fire risk, whereas others may offer higher safety but require longer evacuation distances or longer evacuation times.

The Pareto solutions are then screened. Using the weighted ideal point method, the first-front Pareto solutions for each node are reduced to two routes, each corresponding to one of the two exits. For example, the candidate evacuation routes from Node 1 to the two exits are (1,2,4,8,12,16,14,15) and (1,2,4,8,12,16,23), respectively, and the same procedure is applied to the other nodes. Linear programming is then used to optimize the assignment of evacuees to exits in the overall evacuation route planning, so that the number of evacuees assigned to each exit satisfies the assembly station capacity constraints. Finally, under the combined effects of multiple dynamic factors, such as risk changes caused by fire spread, route traffic capacity, and evacuee movement speed, and by comprehensively considering the objectives of evacuation time, evacuation distance, and fire risk, the representative route selected from the optimal solution set obtained by the multi-objective optimization algorithm is defined as the optimal evacuation route. The resulting optimal evacuation routes from each origin node to the safety exits, together with the corresponding evacuation time, evacuation route length, and fire risk, are presented in Table 9.

Table 9. The optimal evacuation route from each node to the safety exit.

Node ID	Optimal Evacuation Route	Evacuation Time	Route Length	Fire Risk
1	(1,2,4,8,12,16,14,15)	84.774	95.174	2.451
2	(2,9,8,12,10,14,15)	60.998	74.105	2.379
3	(3,7,10,14,15)	88.796	58.796	2.473
4	(4,8,12,10,14,15)	61.854	69.507	2.149
5	(5,1,2,4,8,12,16,14,15)	99.691	79.581	2.382
6	(6,5,1,2,4,8,12,16,14,15)	80.815	94.895	2.895
7	(7,10,14,15)	77.440	47.459	1.991
8	(8,12,10,14,15)	57.585	58.185	1.782
9	(9,8,12,10,14,15)	57.236	63.686	2.171
10	(10,14,15)	36.403	13.898	1.024
11	(11,10,14,15)	31.442	18.934	1.139
12	(12,16,23)	29.698	12.955	1.062
13	(13,12,10,14,15)	34.018	29.838	1.248
14	(14,16,23)	28.105	15.626	1.002
15	-	-	-	-
16	(16,23)	9.625	4.9000	1.005
17	(17,14,15)	41.831	25.326	1.007
18	(18,16,23)	35.230	24.197	1.002
19	(19,18,16,14,15)	54.948	52.941	1.009
20	(20,19,18,16,23)	60.425	62.686	1.001
21	(21,20,19,18,16,23)	78.212	88.661	1.003
22	(22,19,18,16,14,15)	80.909	93.176	1.002
23	-	-	-	-

5.2.3. Comparison of Algorithmic Efficiency

In complex network environments, the efficiency of route planning algorithms directly affects network performance and stability. The time complexity of the improved ant colony optimization algorithm proposed in this study mainly consists of ant path construction,

objective function calculation, and non-dominated sorting. Let I denote the maximum number of iterations, M denote the number of ants, and N denote the number of nodes in the evacuation network. Therefore, the overall time complexity of the proposed algorithm can be expressed as O (I (MN^2 + M^2)).

Furthermore, to assess the effectiveness of various algorithms under networks of different scales, this study conducts comparative experiments on three algorithms, namely the improved ant colony optimization algorithm, a dynamic adjustment algorithm based on Dijkstra's algorithm (DABD) proposed in Hou Shuai's study [36], and the fruit fly optimization algorithm (FOA) [42]. With respect to the number of network nodes, the ship considered in this study has 23 nodes, which already corresponds to a medium-sized passenger ship. Therefore, the second group was set to 40 nodes to simulate the scale of a large passenger ship. In the experiments, the number of network nodes and the number of evacuees were varied, and each group of data was run multiple times at random to obtain the average runtime of each algorithm. The unit of time was set to seconds. The comparison of the computational efficiency of the three algorithms is presented in Table 10.

Table 10. Algorithm operation efficiency comparison.

Network Scale Parameters		Algorithm Efficiency/s		
Network Nodes	**Number of Evacuees**	**Improved ACO**	**FOA**	**DABD**
20	50	0.78121	0.76879	1.14361
20	150	0.84953	1.87345	1.10868
20	300	1.25889	2.45548	1.25982
40	100	1.17187	1.10445	2.97435
40	150	1.88834	2.15078	3.21148
40	400	2.45648	3.25416	3.34879

Note: The DABD algorithm did not take the number of evacuees into account in the experiments.

As shown in Table 10, under six scenarios with different numbers of network nodes and evacuees, the running time of the DABD algorithm is 46.39%, 30.51%, 0.07%, 153.81%, 70.07%, and 36.32% higher than that of the improved ant colony optimization algorithm, respectively. Under a fixed number of network nodes, as the number of evacuees increases, the difference in running time between the DABD algorithm and the improved ant colony optimization algorithm becomes smaller. In addition, the running time of the DABD algorithm is generally positively correlated with the number of network nodes, but does not increase with the number of evacuees. This is because the DABD algorithm does not consider the number of evacuees at each node during route planning; instead, it plans evacuation routes only based on the fire risk section data of each road segment at a given moment. This also indicates that the algorithm has certain limitations.

When the number of network nodes is 20, as the number of evacuees increases from 50 to 150 and then to 300, the running time of the fruit fly optimization algorithm increases by 143.69% and 219.40%, respectively, whereas that of the improved ant colony optimization algorithm increases by only 8.75% and 61.15%, respectively. When the number of network nodes is 40, as the number of evacuees increases from 100 to 150 and then to 400, the running time of the fruit fly optimization algorithm increases by 94.74% and 194.64%, respectively, whereas that of the improved ant colony optimization algorithm increases by only 61.14% and 109.62%, respectively. It can be seen that the running time of the fruit fly optimization algorithm increases rapidly as the number of evacuees grows, indicating that its computational efficiency decreases when dealing with more complex scenarios. This may be because the search mechanism of the fruit fly optimization algorithm relies on random search and local optimization, making it difficult to quickly find the optimal solution

in complex scenarios and thereby increasing the computational time. In contrast, the improved ant colony optimization algorithm can guide the path search through pheromone information. In small-scale problems, such as the scenario with 20 nodes and 50 evacuees, its running time is almost the same as that of the fruit fly optimization algorithm, with a difference of only 0.01 s. Moreover, it can still maintain relatively high computational efficiency in large-scale evacuation problems on large passenger ships. This indicates that the improved ant colony optimization algorithm has certain advantages in terms of efficiency.

5.2.4. Parameter Sensitivity Analysis

In the ant colony optimization algorithm, the relatively sensitive parameters are the heuristic factor β and the pheromone evaporation coefficient ϱ. To analyze the effects of β and ϱ on the solution performance of the improved ant colony optimization algorithm, a one-factor-at-a-time sensitivity analysis was conducted in this study. Under the condition that all other parameters of the original algorithm remained unchanged, the values of β and ϱ were varied separately, and the evacuation time, evacuation distance, and fire risk under different parameter settings were recorded. Taking Node 5 as an example, the results under different parameter values are shown in Tables 11–13.

Table 11. Parameter Sensitivity Analysis of Evacuation Time.

Parameter \ Rate of Change	−50%	−25%	0	25%	50%
β	99.3585	99.6914	99.6914	99.6914	101.6085
ϱ	99.6914	99.6914	99.6914	99.6914	99.3585

According to the results presented in Tables 11–13, the improved ant colony optimization algorithm is generally insensitive to variations in the heuristic factor β and the pheromone evaporation coefficient ϱ, indicating that the algorithm has good parameter robustness. Taking the 0% rate of change as the baseline, the baseline evacuation time, path length, and fire risk are 99.6914 s, 79.5808 m, and 2.3816, respectively.

Table 12. Parameter Sensitivity Analysis of Path Length.

Parameter \ Rate of Change	−50%	−25%	0	25%	50%
β	79.4482	79.5808	79.5808	79.5808	80.3448
ϱ	79.5808	79.5808	79.5808	79.5808	79.4482

Table 13. Parameter Sensitivity Analysis of Fire Risk.

Parameter \ Rate of Change	−50%	−25%	0	25%	50%
β	2.4753	2.3816	2.3816	2.3816	2.1493
ϱ	2.3816	2.3816	2.3816	2.3816	2.4753

In terms of evacuation time, when β varies within the range of −25% to +25%, the evacuation time remains unchanged at 99.6914 s, showing no significant variation. When β decreases by 50%, the evacuation time slightly decreases to 99.3585 s, whereas when β increases by 50%, the evacuation time increases to 101.6085 s, with a maximum increase of approximately 1.92%. The influence of ϱ on evacuation time is even smaller. The evacuation time only decreases to 99.3585 s when ϱ increases by 50%, while it remains unchanged

under the other parameter settings. This indicates that evacuation time is insensitive to changes in both parameters.

In terms of path length, when β varies within the range of −25% to +25%, the path length remains stable at 79.5808 m. When β decreases by 50%, the path length slightly decreases to 79.4482 m, whereas when β increases by 50%, the path length increases to 80.3448 m, with a maximum variation of approximately 0.96%. The influence of ϱ on path length is also weak, with the path length decreasing to 79.4482 m only when ϱ increases by 50%. Therefore, the path length remains generally stable.

In terms of fire risk, the risk value is relatively more sensitive to parameter variations. When β increases by 50%, the fire risk decreases from the baseline value of 2.3816 to 2.1493, indicating that a larger heuristic factor helps the algorithm search for routes with lower fire risk. However, the evacuation time and path length increase slightly at the same time, reflecting that low-risk routes may require certain time and distance costs. When β decreases by 50%, the fire risk increases to 2.4753, indicating that insufficient heuristic information may weaken the algorithm's ability to search for low-risk routes. When ϱ increases by 50%, the fire risk also increases to 2.4753, suggesting that excessive pheromone evaporation may weaken the accumulation of information on high-quality paths and make the algorithm more likely to deviate from low-risk routes.

5.2.5. Comparison of Objective Optimization Performance

To examine the superiority of the proposed dynamic route planning model for passenger ship emergency evacuation and the improved ant colony optimization algorithm in terms of objective optimization performance, the shortest-distance evacuation strategy [43] is selected as the control group. Under this strategy, the evacuation objective is to minimize travel distance, and evacuees are assumed to preferentially choose the evacuation route with the shortest distance from their current location. The resulting shortest evacuation routes from each node to the safety exits, together with the corresponding evacuation time, route length, and route fire risk, are presented in Table 14.

By comparing the simulation results of the proposed optimal evacuation route method in Table 9 with those of the shortest-path method in Table 14, it can be observed that the proposed method achieves better overall evacuation performance under the passenger ship fire scenario. Unlike the shortest-path method, which only minimizes geometric route length, the proposed evacuation route planning model simultaneously considers evacuation time, route length, and fire risk. Therefore, the obtained routes are not necessarily the shortest in distance, but they are more suitable for dynamic fire evacuation conditions.

For Node 1, the evacuation time obtained by the proposed method is 84.774 s, whereas that obtained by the shortest-path method is 105.877 s. The evacuation time is reduced by 21.103 s, corresponding to a decrease of approximately 19.93%. Meanwhile, the fire risk value decreases from 2.732 to 2.451, representing a reduction of approximately 10.29%. Although the route length increases from 63.326 m to 95.174 m, the proposed route avoids road segments with higher fire risk or lower evacuation efficiency, thereby achieving shorter evacuation time and lower fire exposure risk. This result indicates that the shortest geometric path is not necessarily the safest or fastest route in a fire environment.

For Node 5, the proposed method also shows a clear safety advantage. The evacuation time decreases from 101.708 s under the shortest-path method to 99.691 s under the proposed method, with a reduction of 2.017 s. More importantly, the fire risk decreases from 2.885 to 2.382, corresponding to a reduction of approximately 17.44%. This indicates that the proposed method can effectively reduce evacuees' exposure to fire hazards by selecting a safer route, even though the route length increases from 58.204 m to 79.581 m.

In passenger ship fire evacuation, such an increase in route length is acceptable when it leads to a substantial reduction in fire risk.

Table 14. The shortest evacuation route from each node to the safety exit.

Node ID	Shortest Evacuation Route	Evacuation Time	Route Length	Fire Risk
1	(1,3,7,10,14,15)	105.877	63.326	2.732
2	(2,4,8,12,16,23)	62.504	61.998	2.542
3	(3,7,10,14,15)	90.359	58.796	2.473
4	(4,8,12,16,23)	57.504	57.853	2.325
5	(5,6,7,10,14,15)	101.708	58.204	2.885
6	(6,7,10,14,15)	97.257	53.694	2.569
7	(7,10,14,15)	79.003	47.459	1.991
8	(8,12,16,23)	52.2937	46.516	1.782
9	(9,8,12,16,23)	52.885	52.032	2.351
10	(10,14,15)	38.966	13.898	1.212
11	(11,10,14,15)	34.005	18.934	1.139
12	(12,16,23)	31.261	12.955	1.062
13	(13,12,16,23)	28.726	18.169	1.244
14	(14,15)	13.978	5.843	1.009
15	-	-	-	-
16	(16,23)	11.188	4.9	1.005
17	(17,14,15)	44.394	25.326	1.007
18	(18,16,23)	37.793	24.197	1.002
19	(19,18,16,23)	57.511	52.941	1.008
20	(20,19,18,16,23)	61.988	62.686	1.001
21	(21,20,19,18,16,23)	79.775	88.661	1.003
22	(22,19,18,16,23)	78.447	81.507	1.001
23	-	-	-	-

For Node 10, the route length obtained by the two methods is the same, both being 13.898 m. However, the evacuation time decreases from 38.966 s to 36.403 s, and the fire risk decreases from 1.212 to 1.024 under the proposed method. This shows that even when the route length remains unchanged, the proposed method can still improve evacuation performance by considering fire risk and dynamic evacuation conditions rather than relying only on static path length.

The results for some nodes further reflect the trade-off relationship among the three optimization objectives. For example, for Node 4, the evacuation time under the proposed method is 61.854 s, which is slightly higher than the 57.504 s obtained by the shortest-path method. However, the fire risk decreases from 2.325 to 2.149, corresponding to a reduction of approximately 7.57%. Similarly, for Node 9, although the evacuation time increases from 52.885 s to 57.236 s, the fire risk decreases from 2.351 to 2.171, with a reduction of approximately 7.66%. These results indicate that the proposed method does not simply pursue the shortest time or shortest distance, but makes a comprehensive trade-off among evacuation efficiency, route length, and fire safety.

From the perspective of overall performance, the proposed method reduces the evacuation time for 15 out of the 21 evaluated source nodes. The sum of evacuation times decreases from 1217.423 s under the shortest-path method to 1190.035 s under the proposed method, corresponding to a reduction of 27.388 s. The maximum evacuation time is also reduced from 105.877 s to 99.691 s, indicating that the proposed method can effectively improve the evacuation performance of the most unfavorable node. In terms of fire risk, the total fire risk value decreases from 34.343 to 33.177, representing an overall reduction of approximately 3.40%. Although the total route length increases, this is mainly because the proposed method actively avoids high-risk or low-efficiency road segments. In the context

of passenger ship fire evacuation, where safety and time are more critical than geometric distance alone, this trade-off is reasonable and meaningful.

Overall, the comparison between Tables 9 and 14 demonstrates that the proposed evacuation route planning model and improved ant colony optimization algorithm have better comprehensive optimization capability than the shortest-path method. The proposed method can reduce evacuation time for most nodes, lower fire risk for key high-risk nodes, and avoid potentially dangerous road segments. Therefore, it provides a more effective and safer evacuation strategy for passenger ship fire scenarios.

Next, this study compares the cumulative numbers of evacuees at each exit. The numbers of evacuees assigned to each exit under the shortest-route strategy and the proposed optimal-route evacuation strategy are shown in Figure 14.

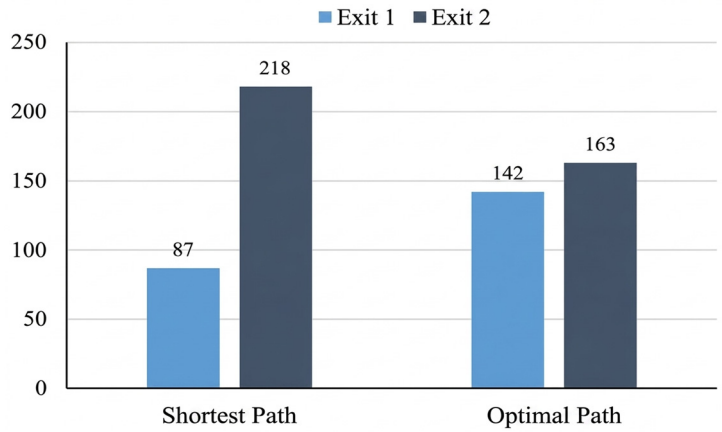


Figure 14. Number of Evacuees at Each Exit under the Shortest-Route and Optimal-Route Evacuation Strategies.

From the figure above, under the shortest-distance evacuation strategy, 218 evacuees are assigned to Exit 23, while only 87 evacuees are assigned to Exit 15. In contrast, under the evacuation strategy proposed in this study, 163 evacuees are assigned to Exit 23, and 142 evacuees are assigned to Exit 15. These results indicate that the proposed passenger ship route planning model satisfies the capacity constraints of the assembly stations while minimizing the overall evacuation cost as much as possible. At the same time, it achieves a more balanced utilization of the safety exits, which is more consistent with real passenger ship conditions and is conducive to improving overall evacuation efficiency.

6. Conclusions

In this study, a personnel evacuation route planning model considering fire spread is established for passenger ship fire scenarios. First, a fire emergency evacuation network for passenger ships is constructed. Second, a dynamic multi-objective optimization model for emergency evacuation routes under passenger ship fire conditions is developed. Then, based on the traditional ant colony optimization algorithm, an improved ant colony optimization algorithm is proposed to solve the multi-objective optimization model. Finally, the RP1 vessel from the publicly available ship evacuation dataset of the SAFEGUARD project under the European Union's Seventh Framework Program is used as an experimental case. Simulation experiments and comparative experiments are conducted to verify the feasibility and effectiveness of the proposed model and algorithm.

However, in terms of constructing the dynamic route planning model for passenger ship fire emergency evacuation, this study still has some limitations. In this study, the real-time number of people in each passage is treated as a deterministic value when analyzing the influence of crowd congestion on real-time walking speed. In practice, however, the

number of people in each passage changes dynamically over time. Therefore, in further research, the number of people in each passage will be characterized as a time-dependent function to further improve the effectiveness of dynamic route planning for passenger ship fire emergency evacuation. With regard to the route optimization strategy, this study is relatively macroscopic and cannot fully reflect certain movement characteristics of evacuees. In further research, personnel evacuation modeling and simulation methods under passenger ship fire scenarios can be further explored, and route optimization strategies that combine microscopic and macroscopic models can be investigated. In terms of the solution algorithm, the proposed algorithm for dynamic route planning in passenger ship fire emergency evacuation still has relatively high computational complexity. Therefore, the algorithm will be further optimized in future research. Due to the limited research time and the author's relatively limited capability, the proposed model still has the above limitations, which requires further in-depth investigation in future studies.

Author Contributions: Conceptualization, K.L.; Methodology, K.L. and C.N.; Software, C.N.; Validation, C.N. and X.L.; Formal analysis, C.N.; Investigation, C.N.; Resources, C.N.; Writing—original draft, X.L.; Writing—review & editing, K.L. and X.L.; Visualization, X.L.; Supervision, K.L.; Project administration, K.L.; Funding acquisition, K.L. All authors have read and agreed to the published version of the manuscript.

Funding: This research was funded by the National Key R&D Program of China (Grant No. 2018YFC0309600\03) and the Fundamental Research Funds for the Central Universities (Grant No. 3132026265).

Data Availability Statement: The original contributions presented in this study are included in the article. Further inquiries can be directed to the corresponding author.

Conflicts of Interest: The authors declare no conflict of interest.

References

1. IMO. Marine Casualties and Incidents. Available online: https://gisis.imo.org/Public/MCIR/Search.aspx (accessed on 1 June 2025).
2. Global Cruise Passengers Carried and Growth Rates, 1990–2024. Available online: https://porteconomicsmanagement.org/pemp/contents/part7_1/ports-and-cruise-shipping/global-cruise-passengers-carried-rates/ (accessed on 22 May 2025).
3. Casareale, C.; Bernardini, G.; Bartolucci, A.; Marincioni, F.; D'Orazio, M. Cruise ships like buildings: Wayfinding solutions to improve emergency evacuation. *Build. Simul.* **2017**, *10*, 989–1003. [CrossRef]
4. Ng, C.T.; Cheng, T.C.E.; Levner, E.; Kriheli, B. Optimal bi-criterion planning of rescue and evacuation operations for marine accidents using an iterative scheduling algorithm. *Ann. Oper. Res.* **2021**, *296*, 407–420. [CrossRef]
5. Xie, Q.; Zhang, S.; Wang, J.; Lo, S.; Guo, S.; Wang, T. A surrogate-based optimization method for the issuance of passenger evacuation orders under ship fires. *Ocean Eng.* **2020**, *209*, 107456. [CrossRef]
6. Li, C.; Hou, J.; Cheng, W.; Gai, W. A multiagent-based modeling approach for emergency evacuation plan optimization during toxic gas releases within chemical plants. *Process Saf. Environ. Prot.* **2022**, *163*, 543–557. [CrossRef]
7. Insani, N.; Akman, D.; Taheri, S.; Hearne, J. Short-notice flood evacuation plan under dynamic demand in high populated areas. *Int. J. Disaster Risk Reduct.* **2022**, *74*, 102844. [CrossRef]
8. Guo, K.; Zhang, L.; Wu, M. Simulation-based multi-objective optimization towards proactive evacuation planning at metro stations. *Eng. Appl. Artif. Intell.* **2023**, *120*, 105858. [CrossRef]
9. Kim, J.; Park, J.; Kim, K.; Kim, M. RnR-SMART: Resilient smart city evacuation plan based on road network reconfiguration in outbreak response. *Sustain. Cities Soc.* **2021**, *75*, 103386. [CrossRef]
10. Khalilpourazari, S.; Pasandideh, S.H.R. Designing emergency flood evacuation plans using robust optimization and artificial intelligence. *J. Comb. Optim.* **2021**, *41*, 640–677. [CrossRef]
11. Chanthakhot, W.; Ransikarbum, K. Integrated computer simulation and data envelopment analysis for fire emergency and evacuation planning in an industrial setting. *J. Ind. Prod. Eng.* **2025**, *42*, 859–875. [CrossRef]
12. Sun, J.; Lu, S.; Lo, S.; Ma, J.; Xie, Q. Moving characteristics of single file passengers considering the effect of ship trim and heeling. *Phys. A Stat. Mech. Its Appl.* **2018**, *490*, 476–487. [CrossRef]

13. Sun, J.; Guo, Y.; Li, C.; Lo, S.; Lu, S. An experimental study on individual walking speed during ship evacuation with the combined effect of heeling and trim. *Ocean Eng.* **2018**, *166*, 396–403. [CrossRef]
14. Chen, J.; Ma, J.; Lo, S.M. Modelling Pedestrian Evacuation Movement on a Swaying Ship. In *Proceedings of the Traffic and Granular Flow '15, Delft, The Netherlands, 28–30 October 2015*; Springer: Berlin/Heidelberg, Germany, 2015; pp. 297–304. [CrossRef]
15. Yang, X.; Zhang, R.; Li, Y.; Pan, F. Passenger evacuation path planning in subway station under multiple fires based on multiobjective robust optimization. *IEEE Trans. Intell. Transp. Syst.* **2022**, *23*, 21915–21931. [CrossRef]
16. Ji, J.; Ma, Z.; He, J.; Xu, Y.; Liu, Z. Research on risk evaluation and dynamic escape path planning algorithm based on real-time spread of ship comprehensive fire. *J. Mar. Sci. Eng.* **2020**, *8*, 602. [CrossRef]
17. Liu, Y.; Zhang, H.; Zhan, Y.; Deng, K.; Dong, L. Evacuation strategy considering path capacity and risk level for cruise ship. *J. Mar. Sci. Eng.* **2022**, *10*, 398. [CrossRef]
18. Liu, L.; Zhang, H.; Shi, J.; Geng, J. Real-time evacuation route optimization in the fire scenarios of cruise ships. *Simul. Model. Pract. Theory.* **2023**, *129*, 102843. [CrossRef]
19. Constantinou, C.; Ellinas, G.; Panayiotou, C.; Polycarpou, M. Shortest Path Routing in Transportation Networks with Time-Dependent Road Speeds. In *Proceedings of the International Conference on Vehicle Technology and Intelligent Transport Systems-Volume 1: VEHITS*; Science and Technology Publications, LDA (SciTePress): Setúbal, Portugal, 2016; pp. 91–98. [CrossRef]
20. Niu, C.; Li, A.; Huang, X.; Li, W.; Xu, C. Research on global dynamic path planning method based on improved A* algorithm. *Math. Probl. Eng.* **2021**, *2021*, 4977041. [CrossRef]
21. Khalid, M.N.A.; Yusof, U.K. Dynamic crowd evacuation approach for the emergency route planning problem: Application to case studies. *Saf. Sci.* **2018**, *102*, 263–274. [CrossRef]
22. Zhang, X.; Zhao, Y.; Deng, N.; Guo, K. Dynamic path planning algorithm for a mobile robot based on visible space and an improved genetic algorithm. *Int. J. Adv. Robot. Syst.* **2016**, *13*, 91. [CrossRef] [PubMed]
23. Men, J.; Chen, G.; Chen, P.; Zhou, L. A Gaussian type-2 fuzzy programming approach for multicrowd congestion-relieved evacuation planning. *IEEE Trans. Intell. Transp. Syst.* **2022**, *23*, 20978–20990. [CrossRef]
24. Wang, W.; Liu, Y.; Xiao, W.; Shang, L. Underwater Target Search Path Planning Based on Sound Speed Profile Clustering and Improved Ant Colony Optimization. *J. Mar. Sci. Eng.* **2025**, *13*, 1983. [CrossRef]
25. Zhang, S.; Yao, J.; Wang, R.; Liu, Z.; Ma, C.; Wang, Y.; Zhao, Y. Design of intelligent fire-fighting robot based on multi-sensor fusion and experimental study on fire scene patrol. *Robot. Auton. Syst.* **2022**, *154*, 104122. [CrossRef]
26. Li, Y.; Tang, C.; Yan, S.; Wang, R.; Gao, D. An Unmanned Vessel Path Planning Method for Floating-Waste Cleaning Based on an Improved Ant Colony Algorithm. *J. Mar. Sci. Eng.* **2025**, *13*, 1579. [CrossRef]
27. Maheshwari, P.; Sharma, A.K.; Verma, K. Energy efficient cluster based routing protocol for WSN using butterfly optimization algorithm and ant colony optimization. *Ad Hoc Netw.* **2021**, *110*, 102317. [CrossRef]
28. Li, Y.; Soleimani, H.; Zohal, M. An improved ant colony optimization algorithm for the multi-depot green vehicle routing problem with multiple objectives. *J. Clean. Prod.* **2019**, *227*, 1161–1172. [CrossRef]
29. Deng, W.; Zhang, L.; Zhou, X.; Zhou, Y.; Sun, Y.; Zhu, W.; Chen, H.; Deng, W.; Chen, H.; Zhao, H. Multi-strategy particle swarm and ant colony hybrid optimization for airport taxiway planning problem. *Inf. Sci.* **2022**, *612*, 576–593. [CrossRef]
30. Dong, K.; Yang, D.; Sheng, J.; Zhang, W.; Jing, P. Dynamic planning method of evacuation route in dam-break flood scenario based on the ACO-GA hybrid algorithm. *Int. J. Disaster Risk Reduct.* **2024**, *100*, 104219. [CrossRef]
31. Liu, L.; Zhang, H.; Xie, J.; Zhao, Q. Dynamic evacuation planning on cruise ships based on an improved ant colony system (IACS). *J. Mar. Sci. Eng.* **2021**, *9*, 220. [CrossRef]
32. Chen, Y.; Miao, Y.; Tao, S.; Li, Q.; Yuan, Y.; Zhang, X.; Hu, L. Flame structure and dynamics in pool fires of different geometries: Experimental and numerical investigation. *Energy* **2024**, *304*, 131996. [CrossRef]
33. Floyd, J.E.; McGrattan, K.B.; Hostikka, S.; Baum, H.R. CFD fire simulation using mixture fraction combustion and finite volume radiative heat transfer. *J. Fire Prot. Eng.* **2003**, *13*, 11–36. [CrossRef]
34. Li, M.; Li, R.; Wang, C. A new-proposed triangular- prism flame radiation model of large-scale spilling fire to subsurface convection flow area. *Process Saf. Environ. Prot.* **2024**, *188*, 1479–1488. [CrossRef]
35. Pichamuthu, J.P. Directional variation of visual range due to anisotropic atmospheric brightness. *Appl. Opt.* **2005**, *44*, 1464–1468. [CrossRef] [PubMed]
36. Guan, W.; Hou, S.; Yu, G.; Gong, H. Dynamic Evacuation Path Planning for Multi-Exit Building Fire: Bi-Objective Model and Algorithm. *Fire Technol.* **2023**, *59*, 2853–2876. [CrossRef]
37. Wattanasaeng, N.; Ransikarbum, K. Sustainable planning and design for eco-industrial parks using integrated multi-objective optimization and fuzzy analytic hierarchy process. *J. Ind. Prod. Eng.* **2024**, *41*, 256–275. [CrossRef]
38. Feliciani, C.; Nishinari, K. Measurement of congestion and intrinsic risk in pedestrian crowds. *Transp. Res. Part C Emerg. Technol.* **2018**, *91*, 124–155. [CrossRef]
39. Liu, Y.; Li, J.; Sun, C. Cellular Automaton Model for Pedestrian Evacuation Considering Impacts of Fire Products. *Fire* **2023**, *6*, 320. [CrossRef]

40. Sun, J.; Lu, Z.; Zhou, D.; Chu, K. Influence of Longitudinal Ventilation Speed on Evacuation Behavior Characteristics Under a Moving Subway Train with Fire. *Fire Technol.* **2025**, *61*, 829–856. [CrossRef]
41. European Commission. SAFEGUARD: Ship Evacuation Data and Scenarios. EU FP7 Project No. 218493. CORDIS Database. Available online: https://cordis.europa.eu/project/id/218493 (accessed on 18 June 2024).
42. Zhang, L.J. Research on Personnel Evacuation Strategies in Complex Building Fires. Ph.D. Thesis, Northeastern University, Shenyang, China, 2019. [CrossRef]
43. Dreyfus, S.E. An appraisal of some shortest-path algorithms. *Oper. Res.* **1969**, *17*, 395–412. [CrossRef]

Disclaimer/Publisher's Note: The statements, opinions and data contained in all publications are solely those of the individual author(s) and contributor(s) and not of MDPI and/or the editor(s). MDPI and/or the editor(s) disclaim responsibility for any injury to people or property resulting from any ideas, methods, instructions or products referred to in the content.